NASA TECHNICAL NOTE

NASA TN D-3048

NASA TN D-3048

FLIGHT PRESSURE DISTRIBUTIONS ON THE VERTICAL STABILIZERS AND SPEED BRAKES OF THE X-15 AIRPLANE AT MACH NUMBERS FROM 1 TO 6

by Jon S. Pyle

Flight Research Center
Edwards, Calif.

NATIONAL AERONAUTICS AND SPACE ADMINISTRATION • WASHINGTON, D. C. • OCTOBER 1965

NASA TN D-3048

FLIGHT PRESSURE DISTRIBUTIONS ON THE VERTICAL STABILIZERS AND SPEED BRAKES OF THE X-15 AIRPLANE AT MACH NUMBERS FROM 1 TO 6

By Jon S. Pyle

Flight Research Center
Edwards, Calif.

NATIONAL AERONAUTICS AND SPACE ADMINISTRATION

For sale by the Clearinghouse for Federal Scientific and Technical Information
Springfield, Virginia 22151 – Price $3.00

FLIGHT PRESSURE DISTRIBUTIONS ON THE VERTICAL STABILIZERS AND SPEED BRAKES OF THE X-15 AIRPLANE AT MACH NUMBERS FROM 1 TO 6

By Jon S. Pyle
Flight Research Center

SUMMARY

Flight pressure distributions are presented for the upper and lower vertical stabilizers of the X-15 airplane with the speed brakes deflected up to 35° at Mach numbers from 1 to 6 and angles of attack from 0° to 15°. Wind-tunnel results agreed well with the flight data. Linear theories provided fair agreement with the flight data when the speed brakes were retracted.

The surface loads on the upper rudder were greatly reduced at the higher angles of attack at supersonic Mach numbers. The speed-brake normal-force and hinge-moment coefficients decreased with increasing Mach number on the upper speed brake. Speed-brake drag, measured from surface pressures in flight, compared favorably with measurements obtained from accelerometers, wind-tunnel force-balance data, and semiempirical estimates.

INTRODUCTION

The X-15 research airplane was designed for flight investigations at supersonic and hypersonic speeds. The structural design required consideration of both thermal and aerodynamic loads under highly transient flight conditions. Therefore, surface-pressure orifices were installed at various locations on the airplane to aid in the analysis of aerodynamic heating and to obtain aerodynamic loads.

This paper, the third in a series (see refs. 1 and 2) on X-15 surface-pressure distributions, presents flight-measured pressure distributions for the upper and lower vertical stabilizers with the speed brakes opened and closed. Data are shown for Mach numbers from 1 to 6 and angles of attack from 0° to 15°. Comparisons are made with wind-tunnel data (refs. 3 and 4) and theory (refs. 5 and 6).

Drag data are also presented for the speed brakes at various deflections at Mach numbers from 1.4 to 5.3 and angles of attack of 5° and 10°. These data are compared with accelerometer measurements (ref. 7), wind-tunnel force-balance data (ref. 8), and semiempirical estimates (refs. 9 and 10).

SYMBOLS

$C_{D_{SB}}$ drag coefficient based on surface area of one speed brake, $C_{N_{SB}} \sin (\delta_{SB} + 5^\circ)$

$C_{h_{SB}}$ hinge-moment coefficient about hinge line of speed brake based on area and chord of one speed brake, $\int_0^1 \left(C_p - C_{p_b}\right) \frac{x'}{c'} d\frac{x'}{c'}$

$C_{N_{SB}}$ normal-force coefficient based on surface area of one speed brake, normal to speed-brake surface, $\int_0^1 \left(C_p - C_{p_b}\right) d\frac{x'}{c'}$

C_p pressure coefficient, $\frac{p - p_\infty}{q} = \frac{p_d + p_r - p_\infty}{q}$

C_{p_b} base pressure coefficient behind speed brake

C_{p_l} pressure coefficient on the lower vertical stabilizer

C_{p_u} pressure coefficient on the upper vertical stabilizer

c local vertical-stabilizer chord, streamwise, ft

c′ local speed-brake chord, streamwise, ft

M free-stream Mach number

p local static pressure, $p_d + p_r$, lb/sq ft absolute

p_d measured differential pressure, $p - p_r$, lb/sq ft

p_r measured reference pressure, lb/sq ft absolute

p_∞ free-stream static pressure, lb/sq ft absolute

q free-stream dynamic pressure, $0.7M^2 p_\infty$, lb/sq ft absolute

x distance rearward of leading edge of local chord parallel to plane of symmetry, ft

x′ distance rearward of speed-brake hinge line parallel to plane of symmetry, ft

z vertical-stabilizer station, measured from fuselage centerline, in.

α airplane angle of attack, deg

Δ root-sum-square error

δ_h horizontal-stabilizer deflection, deg

δ_{SB} speed-brake deflection, deg

δ_v deflection of movable vertical stabilizer, deg

ϵ standard deviation

DESCRIPTION OF AIRPLANE AND MODEL

Airplane

The X-15 airplane (figs. 1 and 2) is a rocket-powered research aircraft designed to attain hypersonic speeds and altitudes in excess of 250,000 feet. A detailed description of the airplane and its control systems is presented in reference 11.

The vertical stabilizers are 10° single-wedge surfaces extending from the upper and the lower surfaces of the fuselage (figs. 1(b) and 3). Each stabilizer has three parts: (1) the stationary base, (2) a pair of speed-brake panels on the rear portion of the stationary base (shown as crosshatched areas in fig. 3) that open to 35°, and (3) a movable portion (rudder) for directional control. The lower rudder is jettisoned for landing.

The horizontal stabilizers (fig. 3), which are used for pitch and roll control, are movable surfaces extending from the side fairings. The root chords of the stabilizers are 3.54 feet from the fuselage centerline. The landing skids (figs. 1(a) and 3) are folded to the exterior surface of the fuselage during flight and are extended before landing. Pertinent dimensions and physical characteristics of the vertical and horizontal stabilizers are presented in table I.

Model

The 0.0667-scale pressure-distribution model of the X-15 used in wind-tunnel tests at the NASA Langley Research Center (refs. 3 and 4) did not have landing skids. The horizontal stabilizer was fixed at a deflection angle of 0°, and the speed brakes could be set at only two positions, 0° and 35°.

INSTRUMENTATION AND ACCURACY

Airplane

The surface-pressure orifices on the X-15 vertical stabilizers (fig. 3) consist of 1/4-inch inner-diameter tubing normal to and flush with the external surface of the skin. Each orifice is connected to standard NACA 24-cell

mechanical-optical manometers by 1/4-inch inner-diameter tubing. Tubing lengths ranged from 5 feet to 20 feet. Since data were obtained under quasi-steady-state flight conditions, the time lag in the system was considered to be negligible, on the basis of the study in reference 12. Because of the limited number of measurements that can be made during a flight, complete coverage of all orifices cannot be shown in each figure. Only one side of the vertical stabilizers were instrumented with pressure orifices.

Surface pressures were measured with differential-pressure cells having a root-mean-square error of ±10 lb/sq ft. The reference pressure (instrument compartment) was measured with absolute-pressure cells having a root-mean-square error of ±6.5 lb/sq ft. These errors were combined by taking the square root of the sum of their squares to give the estimated root-mean-square error in the measured surface pressures. The following estimated errors in other quantities pertinent to this investigation were obtained from reference 13:

Δp_∞, lb/sq ft	$\pm 0.04 p_\infty$
ΔM	±0.07
$\Delta\alpha$, deg	±0.50

The standard deviation in the pressure coefficient ϵC_p (eq. 37 of ref. 14) was determined from the root sum square of each of the individual errors in the measurement

$$\epsilon C_p = \left[\left(\frac{\partial C_p}{\partial p_d}\right)^2 \Delta p_d{}^2 + \left(\frac{\partial C_p}{\partial p_r}\right)^2 \Delta p_r{}^2 + \left(\frac{\partial C_p}{\partial p_\infty}\right)^2 \Delta p_\infty{}^2 + \left(\frac{\partial C_p}{\partial M}\right)^2 \Delta M^2\right]^{1/2} \tag{1}$$

Differentiating $C_p = \dfrac{p_d + p_r - p_\infty}{q}$ with respect to the individual errors and substituting the resulting values into equation (1) gives

$$\epsilon C_p = \left[\left(\frac{1}{q}\right)^2 \left(\Delta p_d{}^2 + \Delta p_r{}^2 + \left(\frac{p_d + p_r}{p_\infty}\right)^2 \Delta p_\infty{}^2 + \frac{4}{M^2}\left(p_d + p_r - p_\infty\right)^2 \Delta M^2\right)\right]^{1/2} \tag{2}$$

The standard deviations in pressure coefficients calculated from equation (2) for a typical low Mach number condition ($M = 1.2$, $\alpha = 10°$, $q = 500$ lb/sq ft) are ±0.05 with the speed brakes closed and ±0.08 with the speed brakes open. At the higher Mach numbers ($M = 2.3$ and 4.7, $\alpha = 15°$, $q = 500$ lb/sq ft), the maximum ϵC_p varies between ±0.03 and ±0.05 with the speed brakes closed and opened, respectively. The values from equation (2) decrease with increasing Mach number and dynamic pressure and increase with increasing angle of attack. Although α does not appear in equation (2), the values of pressure coefficient are dependent upon angle of attack.

Model

The maximum probable error in the wind-tunnel pressure coefficient reported in reference 2 varied from ±0.018 at $M = 2.3$ to ±0.033 at $M = 4.65$.

The maximum deviation in Mach number was ±0.02 at $M = 2.3$ and $M = 2.8$, and ±0.05 at $M = 4.65$. Angle-of-attack and sideslip errors were not presented in references 3 and 4.

TEST CONDITIONS

Airplane

Data were obtained up to an altitude of 100,000 feet ($p_\infty > 20$ lb/sq ft). The data presented herein were chosen from time intervals in which the dynamic pressure was equal to or greater than 500 lb/sq ft, with the exception of Mach numbers below 2.3 for which usable data were limited. To minimize sideslip effects, the data were selected from flight conditions for which the angle of sideslip was less than 1° and the movable rudders were undeflected ($\delta_V = 0°$).

The speed brakes can be opened or closed to any desired angle within 0° to 35°; however, when opened they are usually at maximum deflection (35°). Since the opening rates for the speed brakes are slow, data were obtained at 5° intervals during the opening. The data presented were chosen during the intervals in which the rate of horizontal-stabilizer movement was within 1 deg/sec. The landing skids were folded in flight position, and the lower rudder was attached during all data acquisition.

Model

The wind-tunnel tests with the 0.0667-scale model were conducted in the 8-foot transonic pressure tunnel (ref. 3) and the Unitary Plan tunnel (ref. 4) at the NASA Langley Research Center. The configuration of the model was the same as the flight vehicle with the exception of the landing skids, which were omitted on the model.

The test conditions for both the flight and wind-tunnel data presented herein were as follows:

Wind tunnel			Flight		
M	α, deg	δ_{SB}, deg	M	α, deg	δ_{SB}, deg
1.0	5, 10, 15	0	1.0	5, 10, 15	0
1.2	0, 5, 10	0	1.2	0, 5, 10	0
---	---	--	1.2	5	35
---	---	--	1.4	5, 10	5, 10, 15, 20, 25, 30, 35
---	---	--	1.8	10	5, 10, 15, 20, 25, 30, 35
2.3	0, 5, 10	0	2.3	0, 5, 10	0
2.3	0, 10	35	2.3	0, 5, 10	35
---	---	--	2.5	5	5, 10, 15, 20, 25, 30, 35
3.0	0, 5, 10	0	3.0	0, 5, 10	0
3.0	0, 10	35	3.0	0, 5, 10	35
---	---	--	3.0	5	5, 10, 15, 20, 25, 30, 35
---	---	--	4.0	0, 5, 10	0
---	---	--	4.0	0, 5, 10	35
---	---	--	4.5	5, 10	5, 10, 15, 20, 25, 30, 35
4.7	0, 5, 15	0	4.7	0, 5, 10, 15	0
4.7	15	35	4.7	5, 10, 15	35
---	---	--	5.0	5, 10, 15	0
---	---	--	5.2	5, 10, 15	35
---	---	--	5.3	5	5, 10, 15, 20, 25, 30, 35
---	---	--	6.0	0, 5	0

RESULTS AND DISCUSSION

Pressure Distributions

Pressure distributions on the vertical stabilizers, measured during several X-15 flights, are presented in figures 4 to 6. Data are shown for Mach numbers from 1 to 6 and angles of attack from 0° to 15° with the speed brakes undeflected (δ_{SB} = 0°, figs. 4(a) to 4(h)), partially deflected (δ_{SB} = 30°, fig. 5(b)), and fully deflected (δ_{SB} = 35°, figs. 5(a) and 5(c) to 5(g)). Speed-brake data were obtained at 5° increments while the brakes were being deflected. The data are summarized at four speed-brake positions in figures 6(a) to 6(e). The speed brakes are shown as crosshatched areas when deflected (figs. 5 and 6). The locations of the horizontal stabilizer and landing skids are shown in each figure, since both components have a noticeable effect (discussed later) on the chordwise pressure distributions. Table II presents a complete listing of the analyzed data that were obtained while the speed brakes were being opened.

Wind-tunnel data for the vertical stabilizers (δ_h = 0°, no landing skids) are included in figures 4(a) to (d) and 4(f) and figures 5(c), (d), and (f) for comparison with flight results. The pressure gradients (change of pressure coefficient with chord length) are most prominent at the transonic Mach numbers and when the speed brakes are deflected. The gradients from the model and full-scale vehicle tests compared favorably. The comparison of flight and wind-tunnel pressure-distribution profiles indicates the presence of localized effects due to stabilizer deflection in flight and the addition of the landing skids. The increase in the flight pressure coefficient shown in figure 4(d) (α = 10°, fourth orifice rearward from leading edge on lower stabilizer) is believed to be caused by a shock wave from the landing skids. This effect moves rearward with the increase in Mach number. The upper stations do not experience the effect because of the presence of the side fairing. The interference caused by deflection of the horizontal stabilizer can be seen by the comparison of wind-tunnel results and flight pressure distributions in figure 5(c) (α = 0° and 10°) in the vicinity of the trailing edges of the upper and lower speed brakes. The compression from the upper leading edge of the horizontal stabilizer causes the flight pressures to be greater than the wind-tunnel values on the upper speed brake; whereas, the expansion over the lower leading edge of the horizontal stabilizer causes a reduction in the flight pressures on the lower speed brake. These effects can be seen when the speed brakes are closed, although they are most prominent when the speed brakes are deflected into the fuselage flow field. In view of the differences in configuration between the model and the full-scale vehicle, the pressure coefficients show good agreement.

Summary plots of the basic data of figures 4 and 5 are presented in figures 7(a) to 7(d). Of interest are the increases in pressure coefficient (compressions) over the forward portions of the upper vertical stabilizer at the transonic Mach numbers (figs. 7(a) to 7(c)). These compressions are believed to be caused by shock waves from the horizontal stabilizer and, as shown,

disappear with increasing Mach number. Opening the speed brakes displaced the region of compression rearward.

Comparison With Theory

The locations of the vertical stabilizers on the X-15 airplane make the prediction of pressure distributions on their surfaces difficult. Comparisons of results from two-dimensional (ref. 5) and linear (ref. 6) theories with flight data are shown in figures 8(a) and 8(b) for Mach numbers of 2.3 and 4.7. Linear theory, which considers the effects of the Mach wave interference from the root juncture and stabilizer tip, generally approximates the values measured during flight. However, two-dimensional theory does not account for the Mach wave interference and, therefore, overpredicts the values of the pressure distributions at the root and tip stations. At the midchord, where the flow is nearly two-dimensional, theoretical and experimental results are generally in good agreement. When the speed brakes are deflected (figs. 8(c) and 8(d)), the theories do not give adequate predictions of the pressure distributions over the speed-brake surfaces.

Surface Loads

The effect of speed-brake setting on the chordwise section loads calculated for one side of the vertical stabilizers is shown in figures 9(a) to 9(d). On the tip and midchords (figs. 9(a) and 9(b)), opening the speed brakes does not significantly affect the loading (except at $M = 1.0$, $\alpha = 5°$). The increase in section loads at the transonic Mach numbers is caused by the compressions discussed on page 6 and shown in figures 7(a) and 7(b). The comparison of the opened and the closed speed-brake section loads on the upper and lower root rows (figs. 9(c) and 9(d)) shows large differences due to the change in speed-brake deflection.

The surface pressures on the upper rudder were found to decrease with increasing angle of attack due to the reduced energy of the flow around the rudder, since the rudder is in the flow field of the fuselage and side fairing. At the supersonic Mach numbers, the loss of pressure causes a complete loss of surface load on the upper rudder (fig. 10) and a consequent reduction in the effectiveness of the upper rudder for directional control. To show the reduction in surface loading, wind-tunnel data were used to obtain the ratios shown in figure 10, since there are no surface-pressure orifices on the lower rudder of the full-scale vehicle.

As shown in figure 10, at zero angle of attack the loading on the upper and lower rudders is approximately the same (the ratio of loading varying between 0.8 and 1.2), regardless of the speed-brake setting. However, as angle of attack is increased, the loads on the upper rudder are greatly reduced at the supersonic Mach numbers as a result of the negative pressure coefficients measured on the upper rudder. At the transonic Mach numbers, the compressions near the leading edges (mentioned previously) produce approximately equal upper- and lower-rudder surface loads for the angle-of-attack range of this paper.

Speed-Brake Loads

The speed brakes are basically flat plates deflected into the streamwise flow. By assuming that the spanwise pressure profiles were level across the face of the plate and the base pressure was level across the back (interior) side of the speed-brake section, approximations of the section normal-force and hinge-moment coefficients were obtained as shown in figures 11 and 12, respectively. An increase of the coefficients with speed-brake deflection is noted for each Mach number. Also, a general reduction of the coefficients is evident on the upper speed brake as the Mach number increases; however, the coefficients on the lower speed brake show similar increases at the supersonic Mach numbers.

The increase in incremental drag, calculated from the speed-brake loads, is presented in figure 13 as the speed brakes are deflected into the streamwise flow. Some of these data are compared in figure 14 with accelerometer data from reference 7 and wind-tunnel force-balance data from reference 8. Also shown are semiempirical estimates of drag based on the data in references 9 and 10. The flight-measured surface pressure drag and the accelerometer drag show good agreement and compare favorably with both wind-tunnel force-balance data and semiempirical estimates.

CONCLUSIONS

Measurements of surface pressures over the upper and lower vertical stabilizers of the X-15 airplane at Mach numbers from 1 to 6 and angles of attack from 0° to 15° indicated the following:

1. Pressure gradients from flight and wind-tunnel tests compared favorably. Good agreement was also shown between flight and wind-tunnel pressure-coefficient values.

2. In general, with the speed brakes retracted, fair agreement was obtained between flight-measured surface pressures and linear theory.

3. The surface loads on the upper rudder were greatly reduced at the higher angles of attack and at supersonic speeds.

4. A general reduction of normal-force and hinge-moment coefficients on the upper speed brake was noted as Mach number increased.

5. The drag values derived from flight-measured surface pressures and accelerometer measurements obtained from the speed brakes compared favorably with wind-tunnel force-balance data and semiempirical estimates.

Flight Research Center,
National Aeronautics and Space Administration,
Edwards, Calif., July 30, 1965.

REFERENCES

1. Pyle, Jon S.: Comparison of Flight Pressure Measurements With Wind-Tunnel Data and Theory for the Forward Fuselage of the X-15 Airplane at Mach Numbers From 0.8 to 6.0. NASA TN D-2241, 1964.

2. Pyle, Jon S.: Flight-Measured Wing Surface Pressures and Loads for the X-15 Airplane at Mach Numbers From 1.2 to 6.0. NASA TN D-2602, 1965.

3. Osborne, Robert S.; and Stafford, Virginia C.: Basic Pressure Measurements on a 0.0667-Scale Model of the North American X-15 Research Airplane at Transonic Speeds. NASA TM X-344, 1960.

4. Hodge, B. Leon; and Burbank, Paige B.: Pressure Distribution of a 0.0667-Scale Model of the X-15 Airplane for an Angle-of-Attack Range of 0° to 28° at Mach Numbers of 2.30, 2.88, and 4.65. NASA TM X-275, 1960.

5. Ames Research Staff: Equations, Tables, and Charts for Compressible Flow. NACA Rep. 1135, 1953.

6. Martin, John C.; and Malvestuto, Frank S., Jr.: Theoretical Force and Moments due to Sideslip of a Number of Vertical Tail Configurations at Supersonic Speeds. NACA TN 2412, 1951.

7. Hopkins, Edward J.; Fetterman, David E., Jr.; and Saltzman, Edwin J.: Comparison of Full-Scale Lift and Drag Characteristics of the X-15 Airplane With Wind-Tunnel Results and Theory. NASA TM X-713, 1962.

8. Leupold, Mathias J.; and Freeman, Elizabeth M.: A Second Series of Supersonic Force Tests on the Full-Span Model X-15 for North American Aviation Incorporated. WTR 200, Mass. Inst. of Tech. (Naval Supersonic Laboratory), Sept. 1958.

9. Hoerner, Sighard F.: Fluid-Dynamic Drag. Publ. by the author (148 Busteed Drive, Midland Park, N.J.), 1958.

10. Love, Eugene S.: Base Pressure at Supersonic Speeds on Two-Dimensional Airfoils and on Bodies of Revolution With and Without Fins Having Turbulent Boundary Layers. NACA TN 3819, 1957.

11. Finch, Thomas W.; and Matranga, Gene J.: Launch, Low-Speed, and Landing Characteristics Determined From the First Flight of the North American X-15 Research Airplane. NASA TM X-195, 1959.

12. Saltzman, Edwin J.: Base Pressure Coefficients Obtained From the X-15 Airplane for Mach Numbers Up to 6. NASA TN D-2420, 1964.

13. Larson, Terry J.; and Webb, Lannie D.: Calibration and Comparisons of Pressure-Type Airspeed-Altitude Systems of the X-15 Airplane From Subsonic to High Supersonic Speeds. NASA TN D-1724, 1963.

14. Beers, Yardley: Introduction to the Theory of Error. Second ed., Addison-Wesley Pub. Co., Inc., 1962.

TABLE I

PHYSICAL CHARACTERISTICS OF THE X-15 AIRPLANE

	Upper	Lower
Vertical stabilizers –		
Airfoil section	10° single wedge	10° single wedge
Total area, sq ft	40.91	34.41
Total span, ft	4.58	3.83
Mean aerodynamic chord	8.95	9.17
Root chord, ft	10.21	10.21
Tip chord, ft	7.56	8.00
Length of surface-pressure chords, ft:		
Root	9.75	9.75
Mid	8.65	-----
Tip	7.78	-----
Taper ratio	0.74	0.78
Aspect ratio	0.51	0.43
Sweepback of leading edge, deg	30	30
Sweepback of hinge line, deg	0	0
Sweepback of trailing edge, deg	0	0
Area of control surface, sq ft	26.45	19.95
Deflection of control surface, deg	±7.50	±7.50
Span of control surface, ft	3.13	2.38
Speed brakes, upper and lower:		
Airfoil section	Integral portion of stabilizer	
Total area, sq ft	5.37	
Span, ft	1.46	
Chord, ft	3.38	
Taper ratio	1.00	
Aspect ratio	0.42	
Sweepback of hinge line, deg	0	
Deflection, deg	35	
Horizontal stabilizers –		
Airfoil section	NACA 66005 (modified)	
Total area (includes 63.29 sq ft covered by fuselage), sq ft	115.34	
Span, ft	18.08	
Mean aerodynamic chord, ft	7.05	
Root chord, ft	10.22	
Tip chord, ft	2.11	
Taper ratio	0.21	
Aspect ratio	2.83	
Sweep at 25-percent-chord line, deg	45	
Dihedral, deg	-15	
Ratio horizontal-tail area to wing area	0.58	
Movable surface area, sq ft	51.77	
Deflection:		
Longitudinal, up, deg	15	
Longitudinal, down, deg	35	

TABLE II

TABULATED SURFACE-PRESSURE DATA FOR DEFLECTED SPEED BRAKES

[M = 1.4, $\alpha = 5°$, $\delta_h = -9°$, $\delta_v = 0°$]

z, in.		x/c	C_p on vertical stabilizer						
Upper surface	Lower surface		δ_{SB}, deg						
			5	10	15	20	25	30	35
	-37.5	4	0.41	0.40	0.40	0.42	0.44	0.47	0.49
		15	.31	.31	.28	.29	.32	.37	.38
		21	.18	.16	.14	.13	.15	.20	.31
		32	.18	.18	.18	.20	.18	.16	.17
		48	.08	.08	.07	.07	.10	.06	.09
		53	.07	.07	.06	.07	.07	.12	.15
		59	.02	.02	0	.20	.10	.22	.32
		64	.03	.09	.12	.22	.36	.56	.73
		68	.26	.49	.64	.83	.90	1.03	1.10
		70	.28	.48	.61	.78	.10	1.43	1.70
		77	.24	.32	.44	.59	.75	1.06	1.15
		84	-.05	.11	.20	.40	.49	.81	.95
		97	-.04	.07	.14	.28	.42	.75	.87
37.5		4	-.02	-.04	-.02	-.03	-.01	-.04	-.03
		15	0	-.03	-.01	-.02	-.01	-.02	-.01
		21	0	-.02	-.01	-.02	-.01	-.02	-.02
		32	.06	.05	.05	.08	.04	.04	.05
		48	.11	.10	.10	.11	.13	.16	.20
		53	.13	.13	.09	.16	.25	.35	.48
		59	.15	.15	.16	.24	.46	.76	.85
		64	.19	.19	.35	.53	.66	.82	.90
		68	.37	.62	.72	.83	.93	1.19	1.32
		70	.32	.59	.66	.86	1.03	1.58	1.76
		77	.13	.22	.41	.55	.67	1.06	1.21
		84	.12	.16	.32	.46	.57	.94	1.10
		97	.20	.29	.33	.40	.56	.82	.94
60.5		6	.01	0	0	-.01	-.02	-.03	-.02
		15	.01	.01	.01	-.01	-.02	-.03	-.02
		25	.02	.01	.01	.01	0	.04	.03
		30	.06	.05	.03	.04	.03	.08	.05
		52	.06	.07	.06	.07	.10	.36	.47
		68	.16	.19	.25	.31	.34	.44	.61
		84	.15	.16	.19	.20	.21	.20	.24
		92	.09	.09	.08	.08	.06	.02	.07
78.5		6	.01	0	0	0	-.01	.01	-.01
		15	.01	0	.01	0	.01	.03	.02
		54	.07	.05	0	.02	.08	.27	.32
		72	.15	.15	.18	.21	.25	.32	.45
		90	.13	.13	.15	.15	.16	.18	.20

TABLE II.- Continued

[M = 1.4, α = 10°, δ_h = -12°, δ_v = 0°]

z, in.		x/c	C_p on vertical stabilizer						
Upper surface	Lower surface		δ_{SB}, deg						
			5	10	15	20	25	30	35
	-37.5	4	0.48	0.47	0.48	0.45	0.43	0.44	0.45
		15	.33	.35	.35	.36	.36	.36	.37
		21	.20	.18	.19	.20	.20	.19	.20
		32	.23	.24	.27	.27	.25	.26	.28
		48	.07	.06	.07	.05	.09	.08	.07
		53	.09	.07	.08	.09	.09	.09	.09
		59	.01	.03	.21	.25	.10	.20	.43
		64	.06	.04	.06	.06	.14	.30	.45
		68	.30	.55	.63	.62	.77	.82	.89
		70	.27	.41	.61	.82	.85	1.05	1.22
		77	.18	.24	.38	.43	.62	.77	.91
		84	-.15	-.03	.11	.19	.30	.45	.61
		97	-.02	.02	.11	.21	.34	.42	.53
37.5		4	-.15	-.14	-.15	-.16	-.14	-.15	-.15
		15	-.10	-.09	-.08	-.11	-.09	-.08	-.08
		21	-.10	-.06	-.09	-.11	-.08	-.08	-.09
		32	-.10	-.01	-.12	-.11	-.11	-.11	-.11
		48	.15	.15	.16	.16	.07	.15	.26
		53	.19	.18	.18	.23	.25	.30	.35
		59	.22	.22	.21	.30	.43	.51	.55
		64	.25	.27	.43	.53	.59	.63	.68
		68	.31	.55	.66	.76	.90	.94	.98
		70	.30	.49	.63	.73	.86	1.02	1.24
		77	.19	.31	.42	.55	.65	.77	.89
		84	.10	.17	.27	.41	.54	.63	.72
		97	.03	.11	.28	.39	.46	.53	.60
60.5		6	-.06	-.08	-.06	-.05	-.07	-.06	-.05
		15	-.08	-.09	-.10	-.08	-.07	-.06	-.06
		25	-.06	-.08	-.09	-.08	-.08	-.07	-.06
		30	-.03	-.06	-.06	-.06	-.06	-.06	-.05
		52	.15	.14	.15	.15	.15	.16	.17
		68	.20	.25	.30	.33	.36	.38	.40
		84	.18	.17	.18	.19	.20	.20	.16
		92	-.11	-.10	-.08	-.07	-.06	-.05	-.04
78.5		6	-.06	-.07	-.08	-.06	-.06	-.05	-.04
		15	-.09	-.11	-.10	-.09	-.09	-.08	-.07
		54	.14	.13	.14	.13	.15	.16	.17
		72	.15	.17	.19	.21	.23	.26	.29
		90	.11	.12	.14	.14	.16	.15	.16

TABLE II.- Continued

[M = 1.8, α = 10°, δ_h = -15°, δ_v = 0°]

z, in.		x/c	C_p on vertical stabilizer						
Upper surface	Lower surface		δ_{SB}, deg						
			5	10	15	20	25	30	35
	-37.5	4	0.28	0.29	0.30	0.28	0.25	0.23	0.21
		15	.38	.38	.38	.40	.38	.38	.36
		21	.25	.26	.25	.26	.29	.29	32
		32	.25	.27	.27	.28	.25	.25	.28
		48	.15	.15	.18	.18	.18	.18	.18
		53	.15	.16	.15	.18	.22	.21	.23
		59	.07	.08	.09	.19	.41	.41	.44
		64	.12	.10	.13	.12	.17	.30	.40
		68	.30	.50	.65	.65	.66	.67	.69
		70	.19	.33	.53	.65	.74	.84	.94
		77	.23	.33	.42	.55	.65	.76	1.01
		84	.05	.13	.23	.30	.40	.57	.67
		97	0	.07	.09	.19	.29	.39	.59
37.5		4	-.04	-.04	-.05	-.03	-.07	-.06	-.05
		15	-.05	-.05	-.06	-.07	-.04	-.04	-.05
		21	-.06	-.06	-.07	-.08	-.08	-.04	-.05
		32	-.08	-.07	-.08	-.08	-.08	-.06	-.06
		48	-.06	-.06	-.08	-.07	-.11	-.07	-.09
		53	-.04	-.06	-.05	-.05	-.05	-.04	-.04
		59	0	0	.01	.05	.27	.28	.27
		64	.10	.15	.23	.25	.29	.27	.24
		68	.30	.40	.57	.60	.62	.65	.70
		70	.30	.45	.65	.71	.90	.96	1.04
		77	.26	.40	.61	.73	.83	1.03	1.12
		84	.20	.35	.51	.63	.73	.79	.94
		97	.18	.27	.41	.51	.58	.74	.88
60.5		6	-.02	-.02	-.02	-.03	-.03	-.02	-.01
		15	-.02	-.02	-.03	-.03	-.04	-.03	-.03
		25	-.05	-.04	-.05	-.05	-.05	-.02	-.01
		30	-.07	-.06	-.06	-.07	-.06	-.02	-.01
		52	-.09	-.09	-.09	-.09	-.10	-.09	-.09
		68	.09	.10	.10	.10	.08	.06	.06
		84	.21	.24	.24	.24	.25	.26	.27
		92	-.02	0	.02	.11	.12	.12	.11
78.5		6	0	.01	-.01	.01	0	.02	.03
		15	-.02	-.02	-.04	-.03	-.03	-.03	-.03
		54	-.08	-.08	-.09	-.10	-.10	-.09	-.07
		72	-.02	-.03	-.02	0	.05	.06	.04
		90	.06	.07	.06	.12	.15	.14	.12

TABLE II.- Continued

[M = 2.5, $\alpha = 5°$, $\delta_h = -7°$, $\delta_v = 0°$]

z, in.		x/c	C_p on vertical stabilizer						
Upper surface	Lower surface		δ_{SB}, deg						
			5	10	12	20	25	30	35
	-37.5	4	0.10	0.11	0.12	0.11	0.12	0.14	0.13
		15	.08	.09	.09	.09	.09	.10	.10
		21	.15	.14	.12	.12	.12	.12	.12
		32	.14	.15	.15	.16	.16	.17	.18
		48	.08	.09	.08	.09	.10	.11	.12
		53	.08	.08	.07	.08	.08	.11	.12
		59	.06	.06	.06	.07	.07	.15	.20
		64	.05	.07	.08	.08	.14	.27	.32
		68	.17	.28	.41	.58	.70	.73	.76
		70	.06	.25	.37	.50	.70	.96	1.09
		77	.14	.23	.29	.45	.67	.89	.94
		84	.08	.16	.23	.34	.55	.75	.87
		97	-.03	.03	.14	.20	.34	.51	.80
37.5		4	.05	.06	.03	.04	.01	.03	.03
		15	.04	.04	.02	.02	0	.01	0
		21	.01	.02	0	.01	-.01	-.01	-.01
		32	-.04	-.02	-.02	-.02	-.02	-.02	-.02
		48	-.01	-.03	-.04	-.03	-.04	-.04	-.04
		53	-.01	-.02	-.04	-.04	-.04	-.04	-.04
		59	-.02	-.02	.04	-.04	-.04	-.03	0
		64	-.05	-.05	.03	-.04	0	.16	.20
		68	.09	.12	.26	.32	.34	.42	.50
		70	.10	.32	.39	.40	.47	.70	.82
		77	.05	.17	.30	.36	.47	.84	.96
		84	.04	.14	.28	.32	.47	.76	.88
		97	.05	.12	.25	.33	.48	.74	.80
60.5		6	.04	.04	.05	.04	.04	.05	.05
		15	.04	.04	.05	.04	.04	.05	.05
		25	.04	.05	.06	.04	.03	.05	.05
		30	.04	.05	.06	.04	.05	.06	.05
		52	.01	.01	.01	.01	-.02	0	0
		68	0	0	0	-.01	-.02	-.02	-.01
		84	-.02	0	-.01	-.02	-.02	0	-.01
		92	.03	0	-.02	-.02	-.02	0	-.01
78.5		6	.07	.07	.07	.06	.07	.07	.07
		15	.05	.06	.05	.06	.06	.06	.06
		54	.01	0	0	0	-.02	-.02	-.02
		72	0	0	0	0	-.02	-.02	-.02
		90	0	-.01	-.02	-.02	-.03	-.02	-.02

TABLE II.- Continued

[M = 3.0, $\alpha = 5°$, $\delta_h = -8°$, $\delta_v = 0°$]

z, in.		x/c	C_p on vertical stabilizer						
Upper surface	Lower surface		δ_{SB}, deg						
			5	10	15	20	25	30	35
	-37.5	4	0.13	0.11	0.12	0.11	0.13	0.12	0.12
		15	.09	.09	.07	.07	.08	.08	.07
		21	.09	.11	.09	.08	.09	.10	.08
		32	.15	.16	.14	.13	.16	.16	.16
		48	.09	.10	.07	.07	.10	.07	.10
		53	.07	.08	.06	.06	.08	.10	.13
		59	.06	.06	.05	.05	.07	.14	.34
		64	.10	.06	.05	.07	.14	.15	.17
		68	.14	.32	.50	.54	.60	.68	.74
		70	.07	.19	.31	.47	.64	.73	.94
		77	.28	.40	.45	.55	.93	1.18	1.46
		84	.17	.31	.33	.38	.52	.64	1.17
		97	.07	.10	.19	.24	.40	.54	.75
37.5		4	.03	.03	.05	.04	.05	.06	.03
		15	.04	.04	.05	.04	.05	.04	0
		21	.03	.03	.03	.04	.04	.03	0
		32	.03	.02	.02	.04	.02	.01	0
		48	0	.02	.02	.03	0	0	0
		53	0	.02	.02	.03	0	0	0
		59	0	.02	.02	.03	0	0	0
		64	.02	.01	.02	.03	.04	.14	.12
		68	.07	.10	.22	.30	.37	.43	.53
		70	.07	.22	.27	.42	.53	.62	.65
		77	.03	.12	.23	.37	.59	.69	.83
		84	.03	.10	.21	.34	.47	.66	.75
		97	.04	.08	.17	.24	.46	.59	.65
60.5		6	.06	.06	.06	.07	.06	.06	.05
		15	.05	.06	.06	.07	.06	.06	.03
		25	.08	.08	.06	.08	.07	.07	.05
		30	.10	.10	.09	.09	.09	.10	.05
		52	.02	.04	.03	.05	.03	.03	.01
		68	.02	.03	.03	.05	.03	.03	0
		84	.02	.02	0	.04	.02	.03	.01
		92	.01	.02	-.01	.04	.02	.02	.01
78.5		6	.08	.08	.08	.09	.08	.07	.07
		15	.08	.08	.07	.07	.07	.07	.05
		54	.03	.03	.03	.04	.04	.04	.02
		72	.02	.02	.02	.04	.04	.03	.01
		90	.02	.02	.02	.04	.04	.03	.01

TABLE II.- Continued

[M = 4.5, $\alpha = 5°$, $\delta_h = -5°$, $\delta_v = 0°$]

z, in.		x/c	C_p on vertical stabilizer						
			δ_{SB}, deg						
Upper surface	Lower surface		5	10	15	20	25	30	35
	-37.5	4	0.09	0.10	0.09	0.08	0.09	0.08	0.08
		15	.02	.03	.03	.03	.03	.02	.01
		21	.03	.05	.03	.02	.04	.02	.03
		32	.07	.08	.06	.06	.07	.05	.10
		48	.08	.08	.08	.08	.09	.07	.06
		53	.08	.09	.08	.08	.09	.10	.11
		59	.05	.05	.06	.05	.09	.18	.26
		64	.06	.05	.05	.05	.05	.06	.15
		68	.12	.18	.28	.40	.43	.44	.48
		70	.12	.20	.30	.43	.60	.75	.83
		77	.16	.28	.41	.57	.74	1.09	1.65
		84	.13	.23	.36	.49	.69	.85	1.21
		97	.09	.14	.28	.36	.60	.71	.86
37.5		4	.04	.06	.04	.03	.02	.05	.02
		15	.01	.02	.02	.01	.01	0	.02
		21	0	.01	.01	0	0	0	.02
		32	0	0	0	0	0	0	0
		48	.02	.02	.01	0	0	.01	0
		53	.01	.02	.02	0	0	0	0
		59	.01	.01	.02	0	0	0	0
		64	.01	.01	.02	0	0	.06	.08
		68	.08	.14	.19	.28	.33	.38	.40
		70	.09	.15	.23	.32	.35	.55	.58
		77	.08	.15	.23	.33	.41	.46	.64
		84	.08	.15	.24	.32	.38	.43	.60
		97	.05	.13	.25	.28	.37	.43	.58
60.5		6	.05	.05	.04	.04	.04	.05	.05
		15	.05	.05	.04	.04	.04	.05	.05
		25	.05	.07	.07	.06	.04	.05	.05
		30	.05	.07	.07	.06	.04	.05	.05
		52	.05	.03	.03	.03	.03	.03	.02
		68	.05	.04	.04	.04	.03	.03	.02
		84	.04	.03	.04	.03	.03	.03	.02
		92	.02	.01	.04	-.02	.03	.03	.02
78.5		6	.06	.06	.07	.06	.06	.05	.05
		15	.05	.05	.05	.06	.04	.05	.02
		54	.02	.01	.02	.02	.01	.02	0
		72	.02	.02	.02	.02	.01	.02	0
		90	.02	.01	.02	.02	.01	.02	0

TABLE II.- Continued

[M = 4.5, α = 10°, δ_h = -11°, δ_v = 0°]

z, in.		x/c	C_p on vertical stabilizer						
Upper surface	Lower surface		δ_{SB}, deg						
			5	10	15	20	25	30	35
	-37.5	4	0.12	0.12	0.14	0.14	0.13	0.14	0.15
		15	.03	.02	.03	.04	.03	.04	.03
		21	.04	.04	.04	.06	.05	.04	.06
		32	.08	.07	.10	.11	.10	.10	.11
		48	.10	.11	.13	.11	.12	.11	.15
		53	.14	.14	.16	.15	.14	.15	.18
		59	.06	.06	.09	.08	.10	.09	.10
		64	.08	.08	.10	.10	.12	.20	.38
		68	.12	.21	.34	.48	.59	.62	.65
		70	.06	.16	.35	.51	.73	.84	.90
		77	.20	.30	.47	.69	1.04	1.40	1.94
		84	.15	.25	.47	.64	.92	1.12	1.60
		97	.14	.22	.36	.54	.70	.86	1.11
37.5		4	.03	0	.01	0	0	0	0
		15	.01	-.01	0	0	0	0	-.01
		21	0	-.01	-.01	.03	0	-.01	-.02
		32	-.01	-.02	-.02	.03	-.03	-.02	-.03
		48	-.01	-.01	-.03	.03	-.03	-.03	-.03
		53	-.01	-.03	-.02	.03	-.03	-.03	-.03
		59	-.02	-.02	-.03	.03	-.03	-.03	-.03
		64	-.02	-.02	-.02	.04	-.04	-.02	0
		68	-.03	-.01	.04	.10	.11	.13	.16
		70	.01	.03	.07	.13	.17	.20	.27
		77	.01	.05	.09	.14	.22	.28	.35
		84	.02	.02	.07	.08	.20	.31	.46
		97	.01	.01	.06	.16	.29	.30	.31
60.5		6	.03	.02	.03	.03	.02	.03	.03
		15	.01	0	.01	.01	0	0	.01
		25	.03	.03	.04	.04	.01	.02	.02
		30	.03	.03	.04	.04	.01	.01	.02
		52	.01	0	.01	.01	0	0	-.01
		68	.02	.01	.02	.02	.01	.01	.01
		84	.02	.02	.01	.01	0	0	.01
		92	.02	.02	.01	.01	0	0	.01
78.5		6	.04	.04	.04	.05	.05	.05	.05
		15	.04	.03	.03	.03	.03	.03	.02
		54	.01	.01	.01	.02	0	0	0
		72	.01	.01	.01	.01	0	0	0
		90	.01	0	.01	.01	0	0	0

TABLE II.- Concluded

[M = 5.3, $\alpha = 5°$, $\delta_h = -5°$, $\delta_v = 0°$]

z, in.		$\frac{x}{c}$	C_p on vertical stabilizer						
Upper surface	Lower surface		δ_{SB}, deg						
			5	10	15	20	25	30	35
	-37.5	4	0.08	0.07	0.07	0.07	0.12	0.08	0.06
		15	.03	.03	.02	.02	.03	.02	.03
		21	.03	.03	.02	.03	.06	.02	.04
		32	.04	.05	.03	.04	.06	.04	.04
		48	.05	.06	.04	.05	.06	.07	.05
		53	.05	.06	.04	.05	.04	.05	.04
		59	.02	.03	.02	.02	.02	.02	0
		64	.04	.04	.05	.05	.04	.15	.20
		68	.10	.17	.22	.28	.35	.40	.48
		70	0	.16	.19	.31	.59	.65	.72
		77	.18	.30	.38	.61	.90	1.15	1.52
		84	.14	.26	.34	.53	.82	.96	1.35
		97	.11	.20	.17	.40	.61	.70	.88
37.5		4	.04	.03	.03	.03	.01	.01	.02
		15	.02	.02	.03	.02	.02	.01	.02
		21	.01	.01	.03	.01	.01	.01	0
		32	.01	.02	.01	.02	.01	.01	0
		48	.01	.02	.01	.02	0	0	0
		53	.01	.02	.01	.02	0	0	0
		59	.01	.02	.01	.02	0	0	0
		64	.01	.02	.04	.05	.05	.03	.01
		68	.04	.11	.11	.22	.28	.32	.40
		70	.05	.11	.15	.24	.28	.39	.50
		77	.06	.11	.19	.26	.30	.40	.50
		84	.07	.11	.19	.26	.30	.40	.50
		97	.07	.13	.18	.26	.30	.40	.50
60.5		6	.03	.04	.04	.03	.04	.03	.03
		15	.02	.04	.04	.03	.04	.03	.03
		25	.04	.04	.03	.03	.04	.03	.03
		30	.04	.04	.03	.03	.07	.03	.03
		52	.03	.04	.03	.03	.02	.03	.01
		68	.04	.04	.03	.03	.02	.03	.01
		84	.04	.04	.03	.03	.02	.03	.01
		92	.04	.04	.03	.03	.03	.03	.01
78.5		6	.06	.07	.07	.06	.06	.05	.04
		15	.06	.06	.07	.06	.06	.05	.05
		54	.02	.01	.01	.01	.02	.03	0
		72	.02	.03	.04	.03	.02	.03	.01
		90	.02	.04	.04	.02	.02	.03	.02

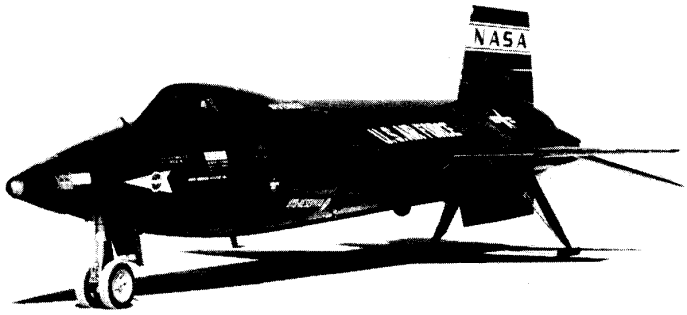

E-7902

(a) Lower ventral stabilizer removed and landing gear down.

E-9908

(b) Rear side view of the vertical stabilizers with the lower ventral stabilizer removed.

Figure 1.– X-15 airplane.

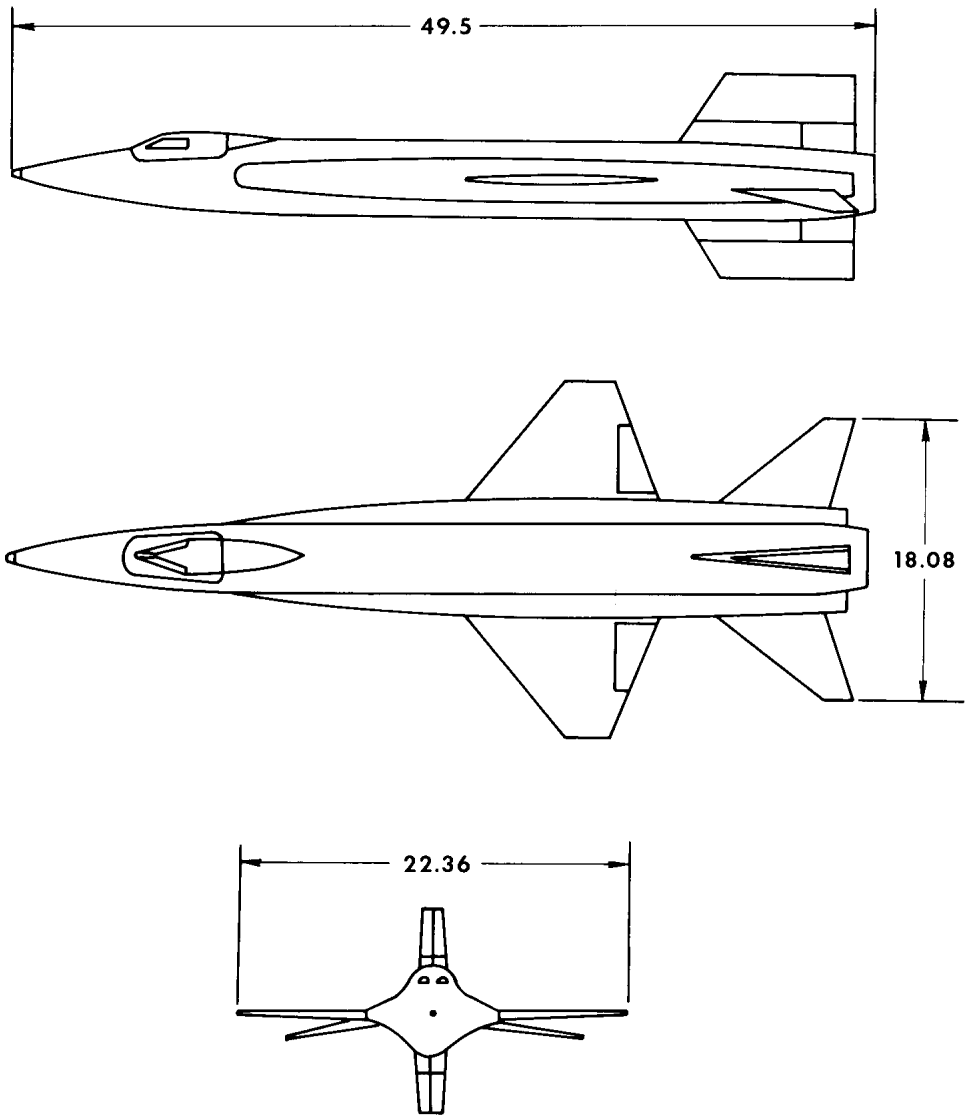

Figure 2.– Three-view drawing of X-15 airplane. Dimensions in feet.

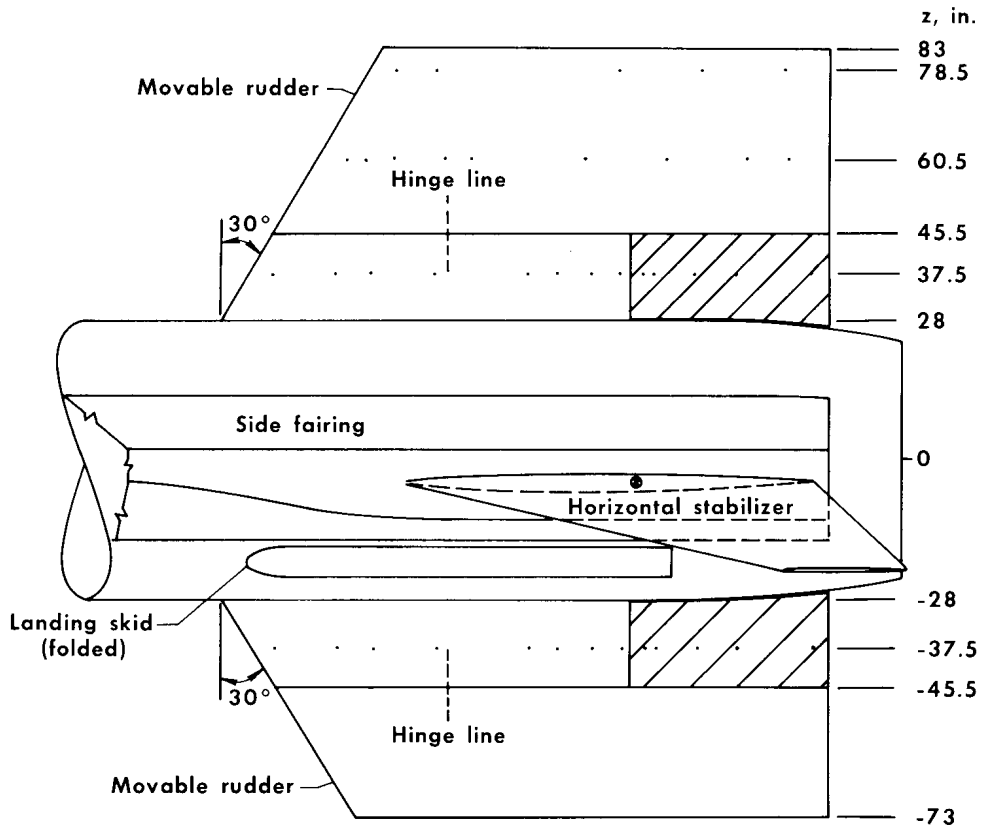

Figure 3.— Orifice locations on the upper and the lower vertical stabilizers.

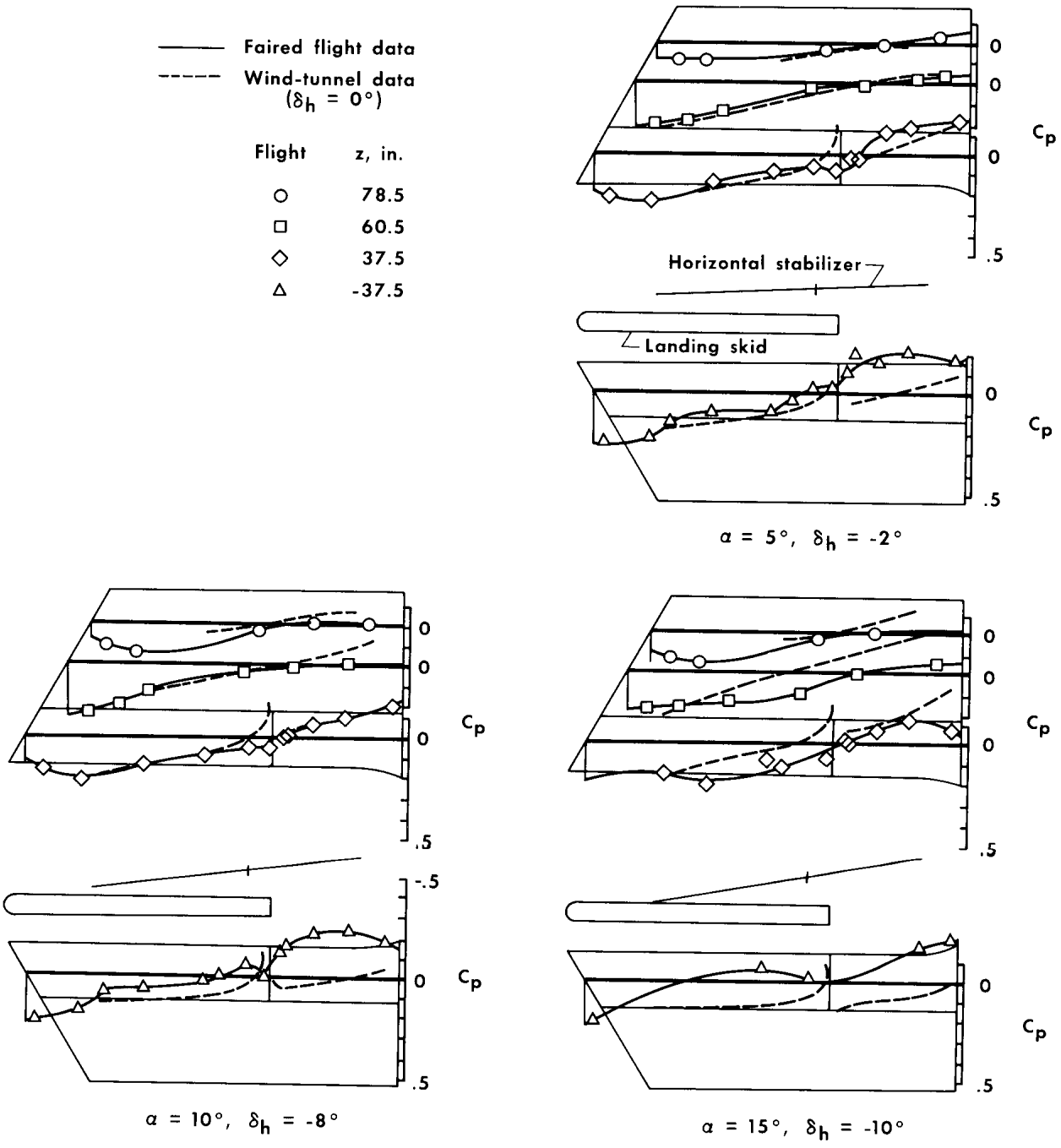

(a) M = 1.0, δ_{SB} = 0°.

Figure 4.– Surface pressures on the X-15 vertical stabilizers. Speed brakes closed.

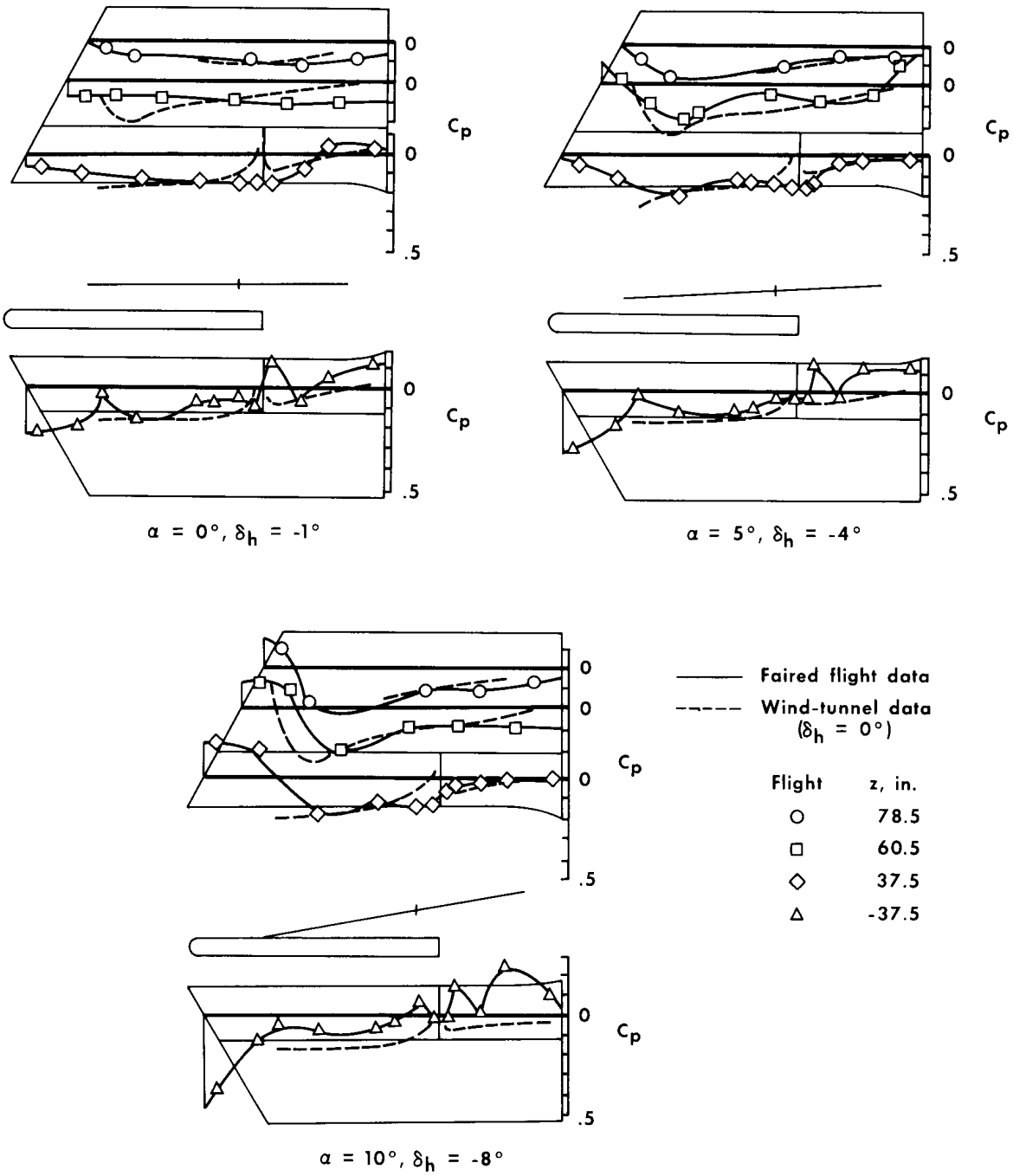

(b) M = 1.2, δ_{SB} = 0°.

Figure 4.– Continued.

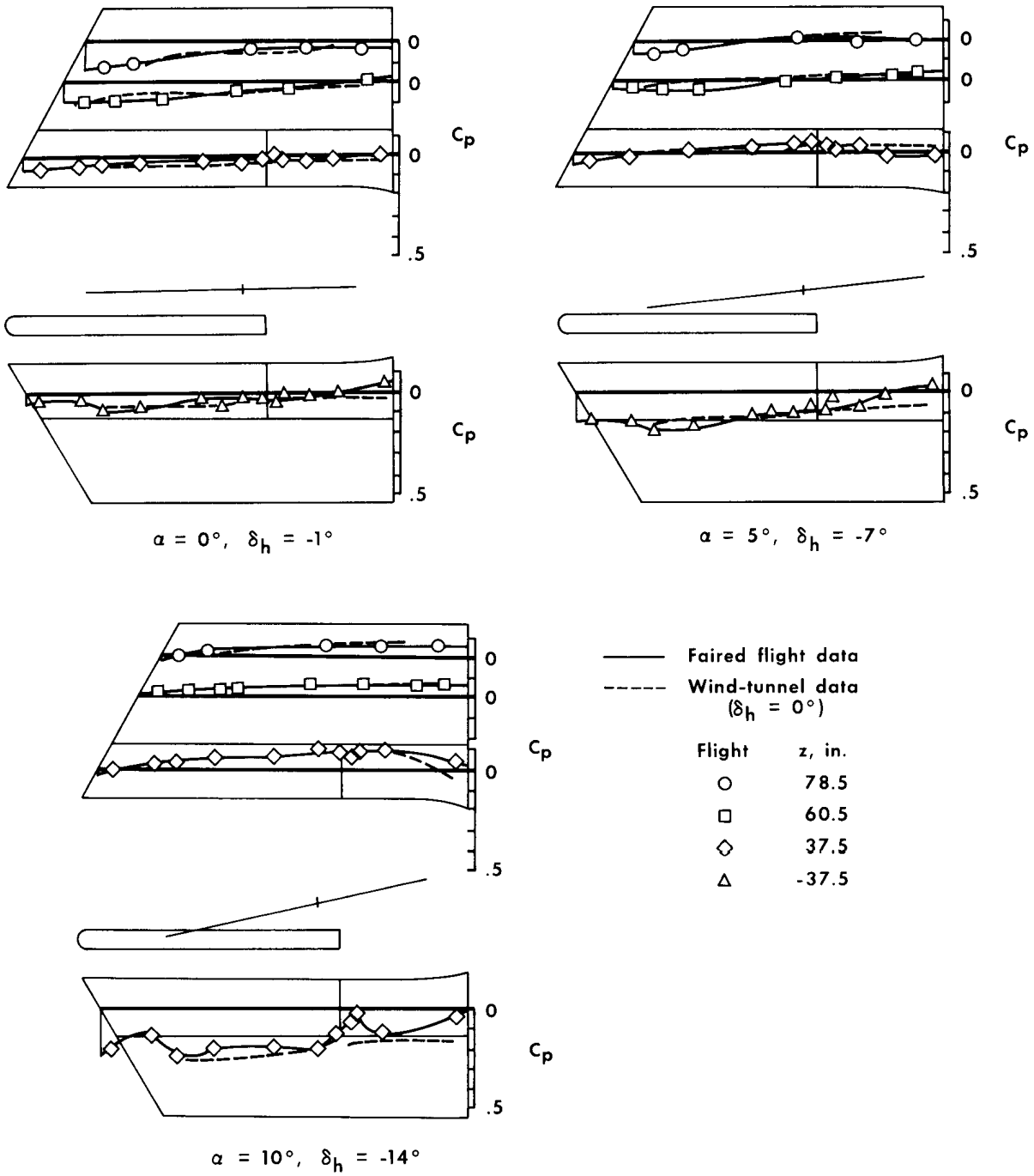

(c) M = 2.3, δ_{SB} = 0°.

Figure 4.– Continued.

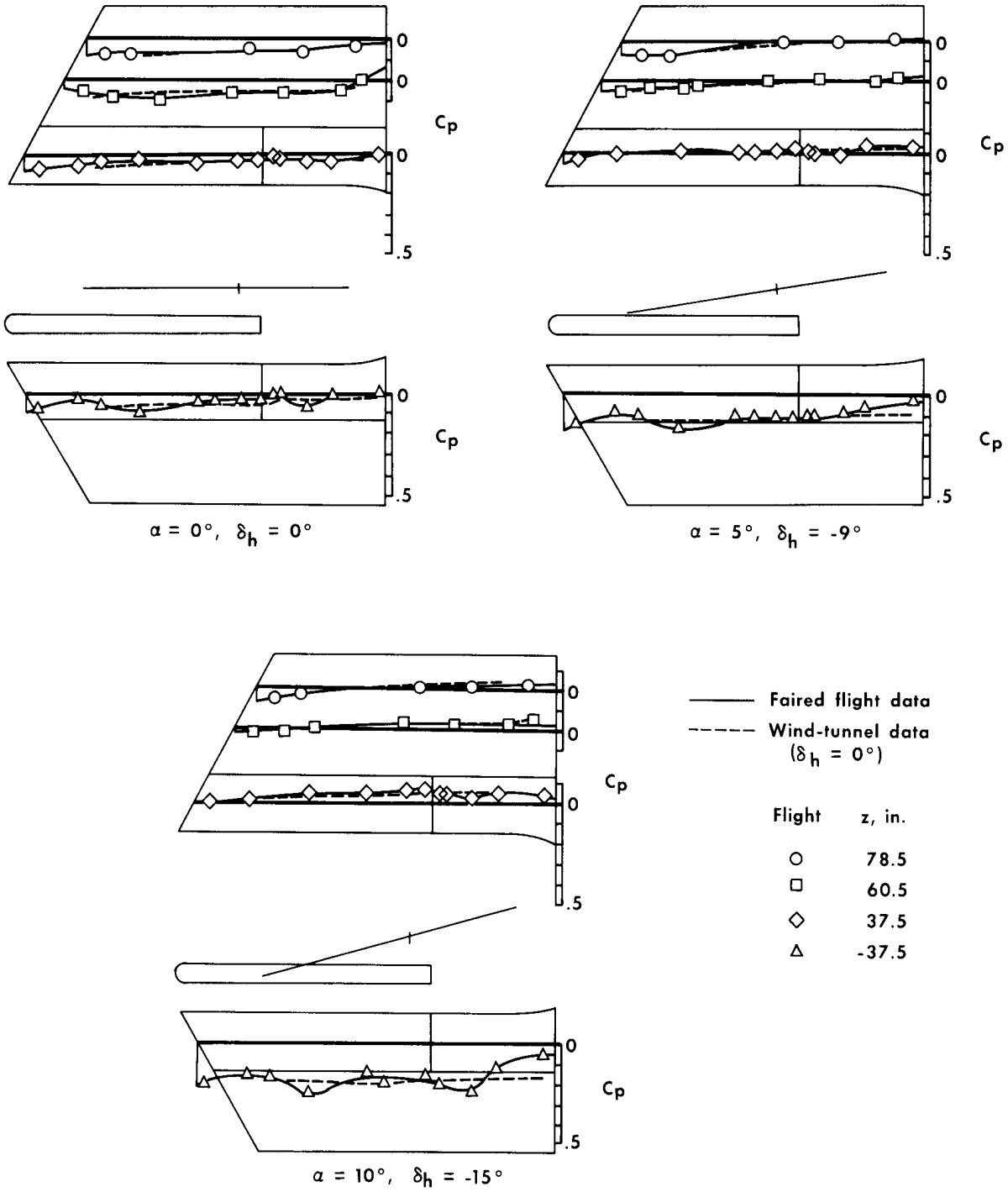

(d) M = 3.0, $\delta_{SB} = 0°$.

Figure 4.– Continued.

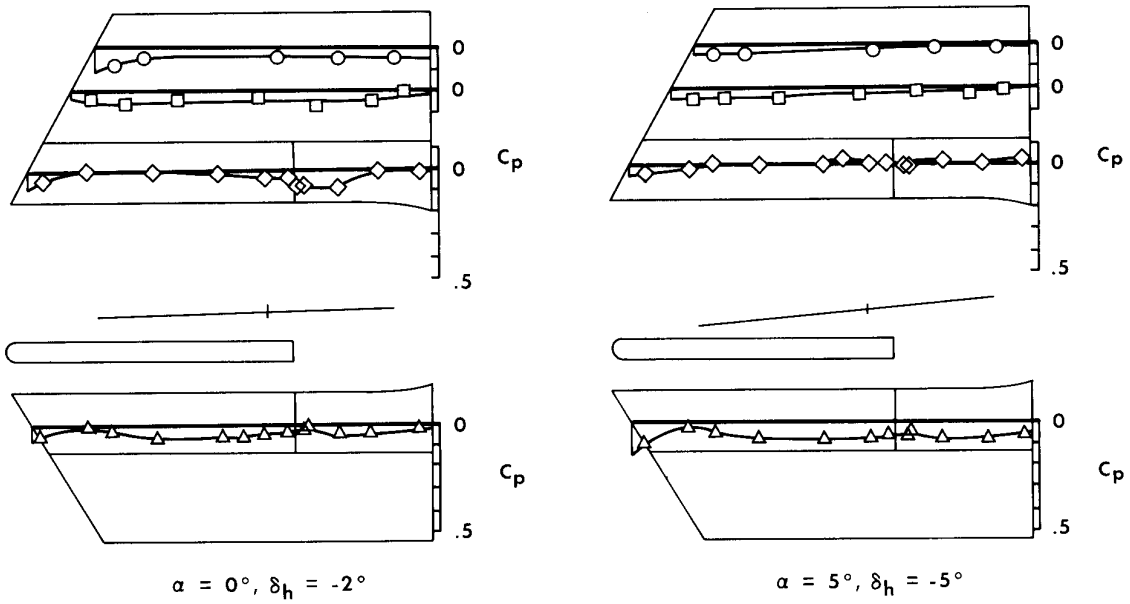

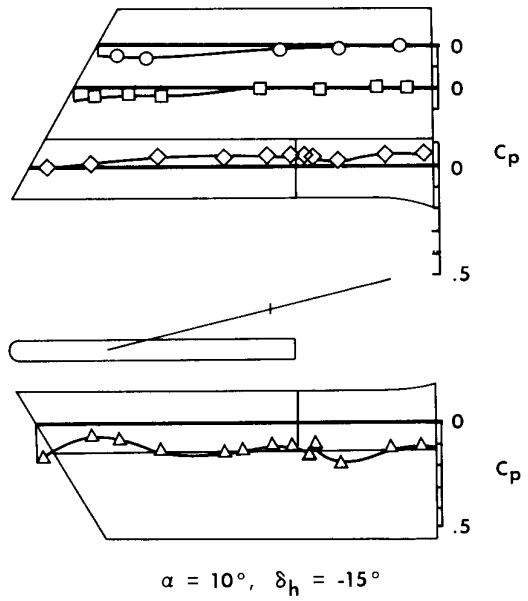

Faired flight data

Flight	z, in.
○	78.5
□	60.5
◇	37.5
△	-37.5

(e) M = 4.0, δ_{SB} = 0°.

Figure 4.– Continued.

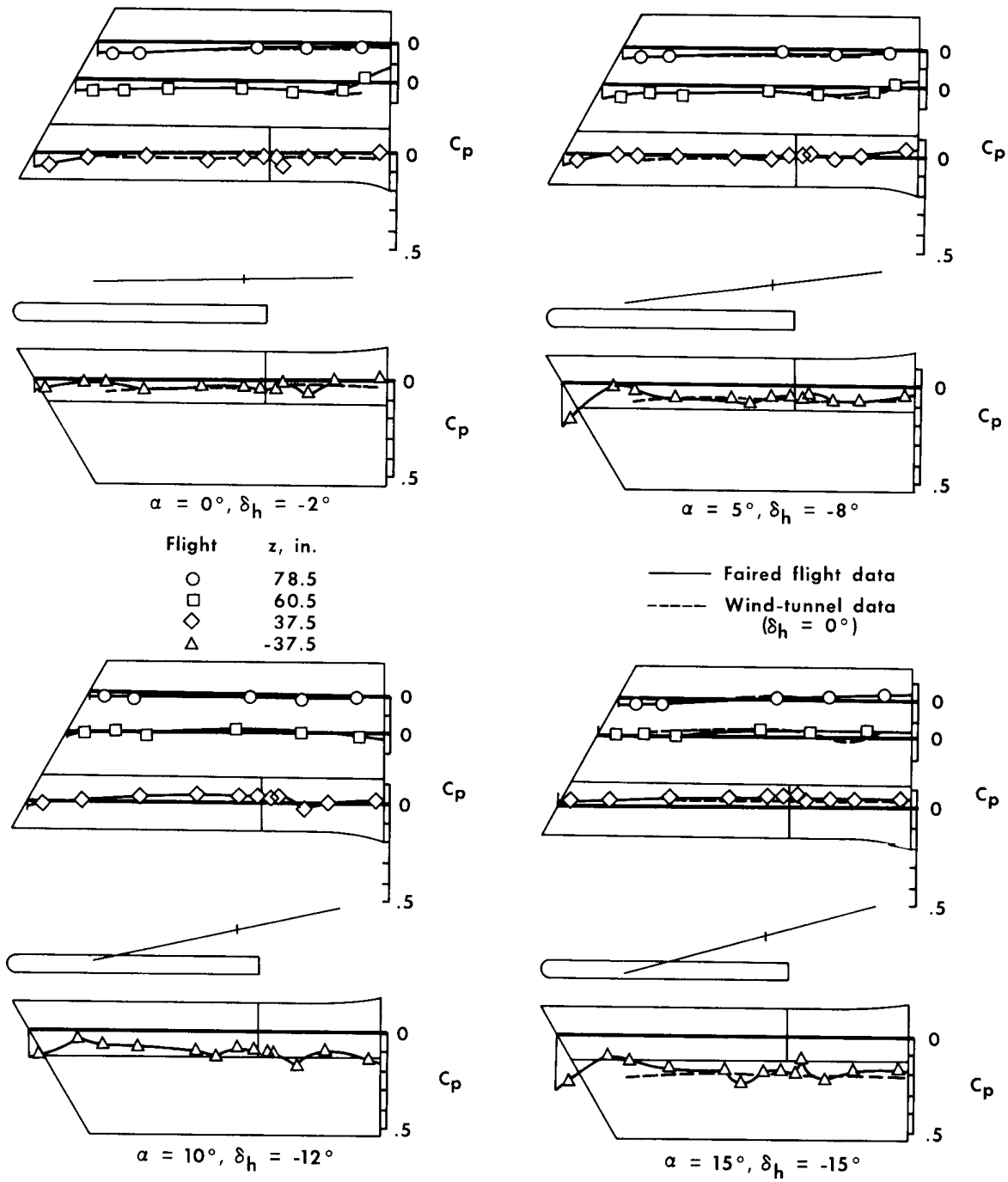

(f) M = 4.7, δ_{SB} = 0°.

Figure 4.- Continued.

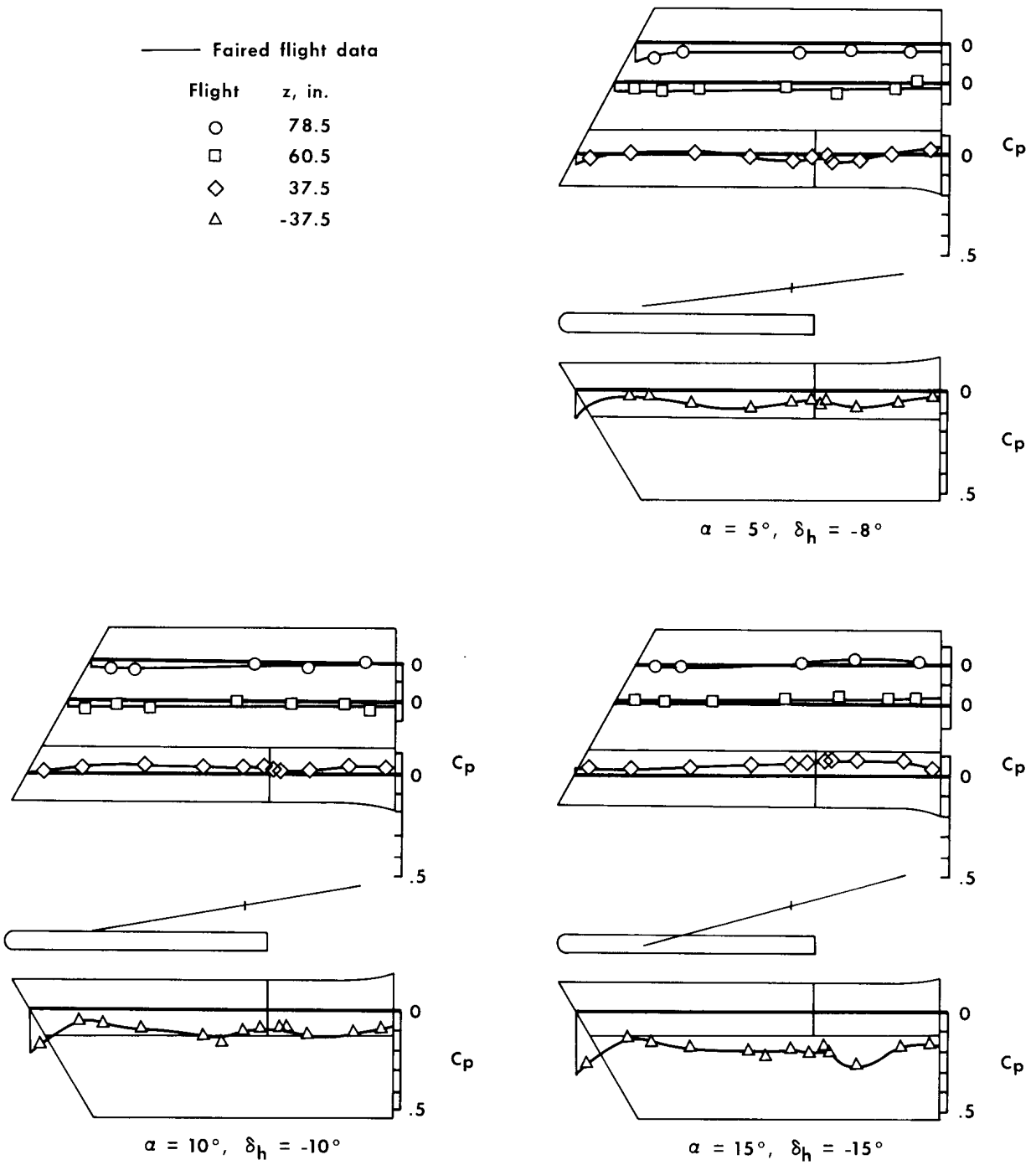

(g) M = 5.0, δ_{SB} = 0°.

Figure 4.– Continued.

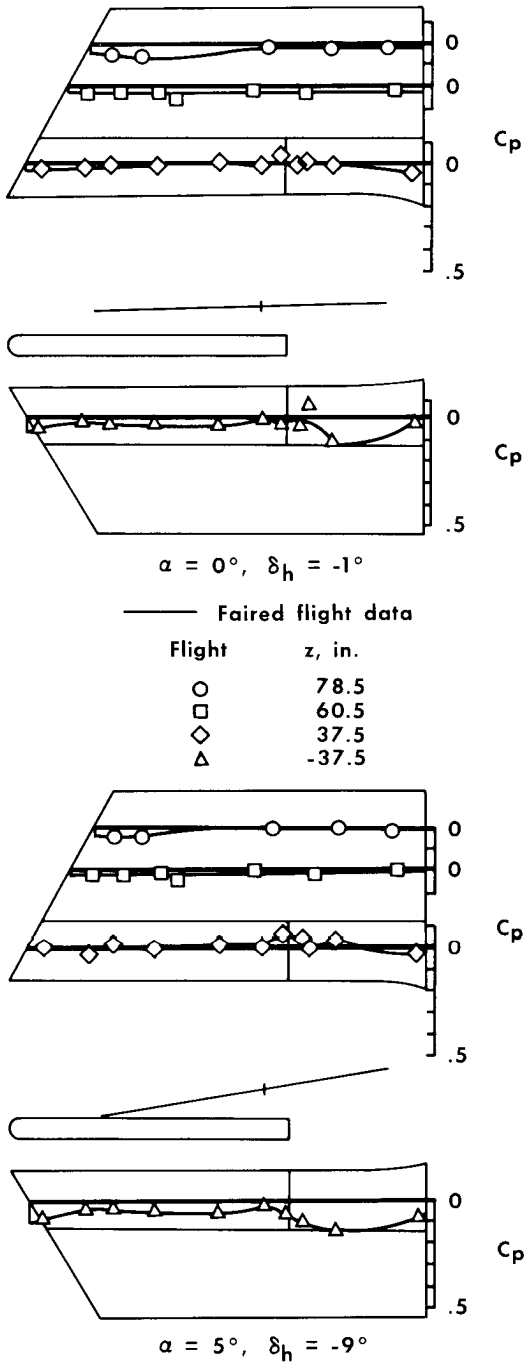

(h) M = 6.0, $\delta_{SB} = 0°$.

Figure 4.– Concluded.

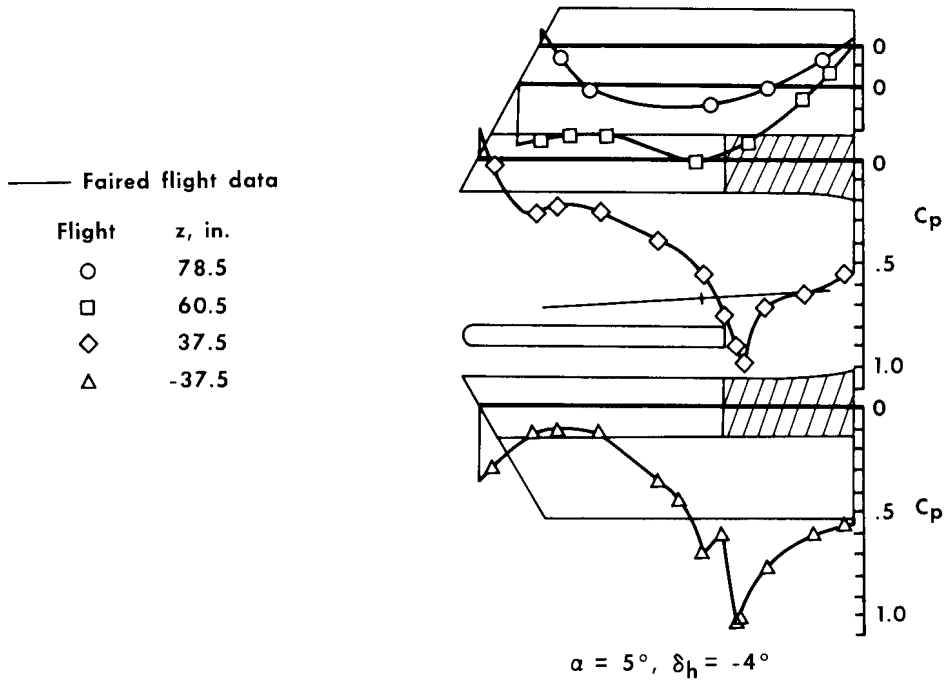

(a) M = 1.2, δ_{SB} = 35°.

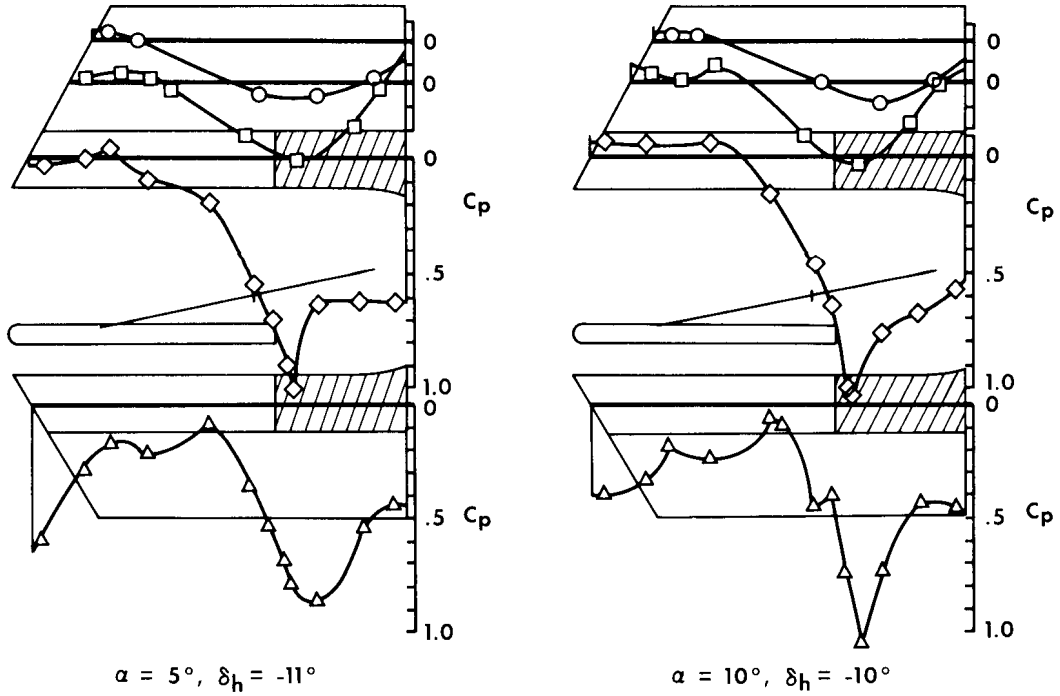

(b) M = 1.4, δ_{SB} = 30°.

Figure 5.– Surface pressures on the vertical stabilizers. Speed brakes extended.

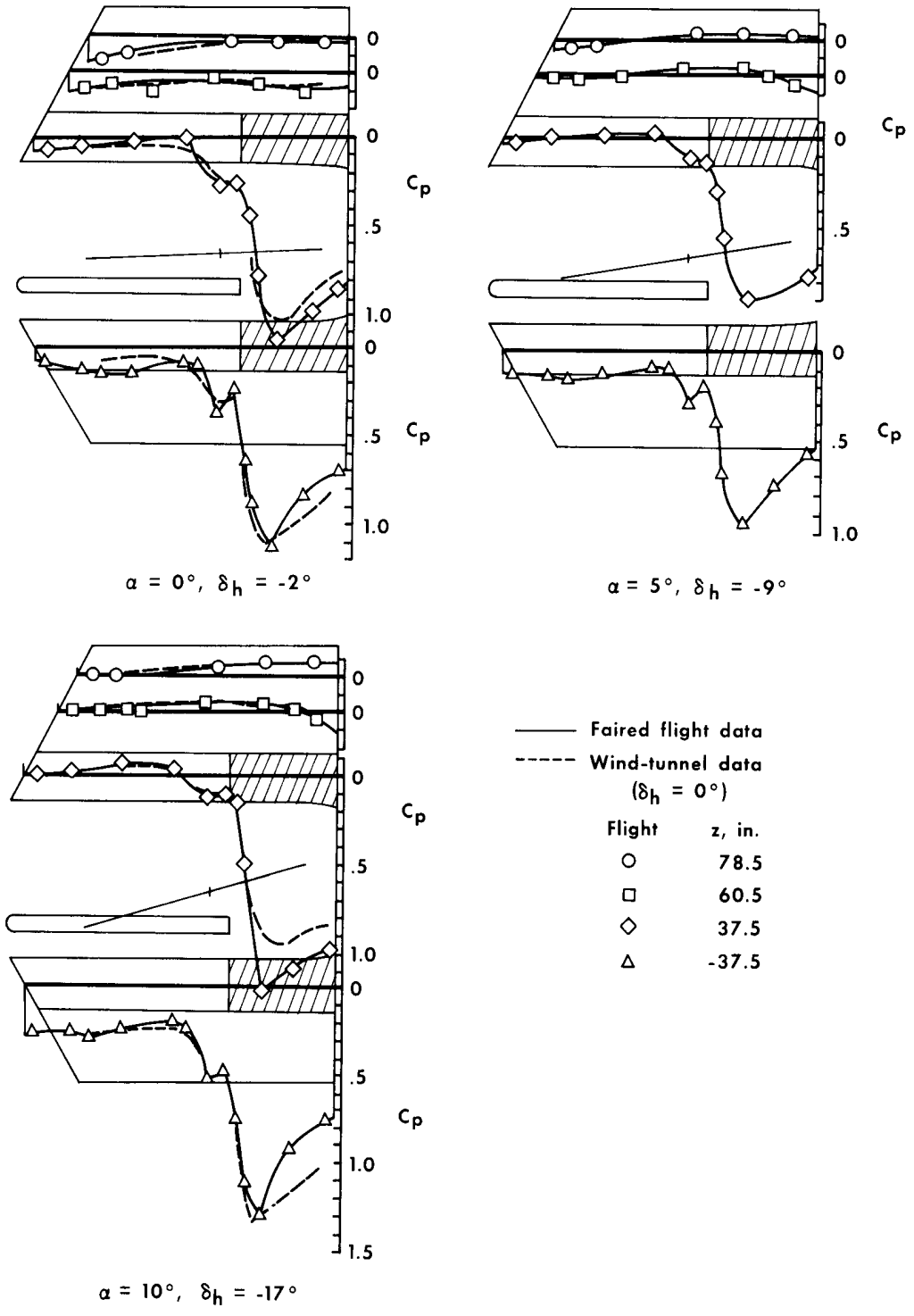

(c) M = 2.3, δ_{SB} = 35°.

Figure 5.– Continued.

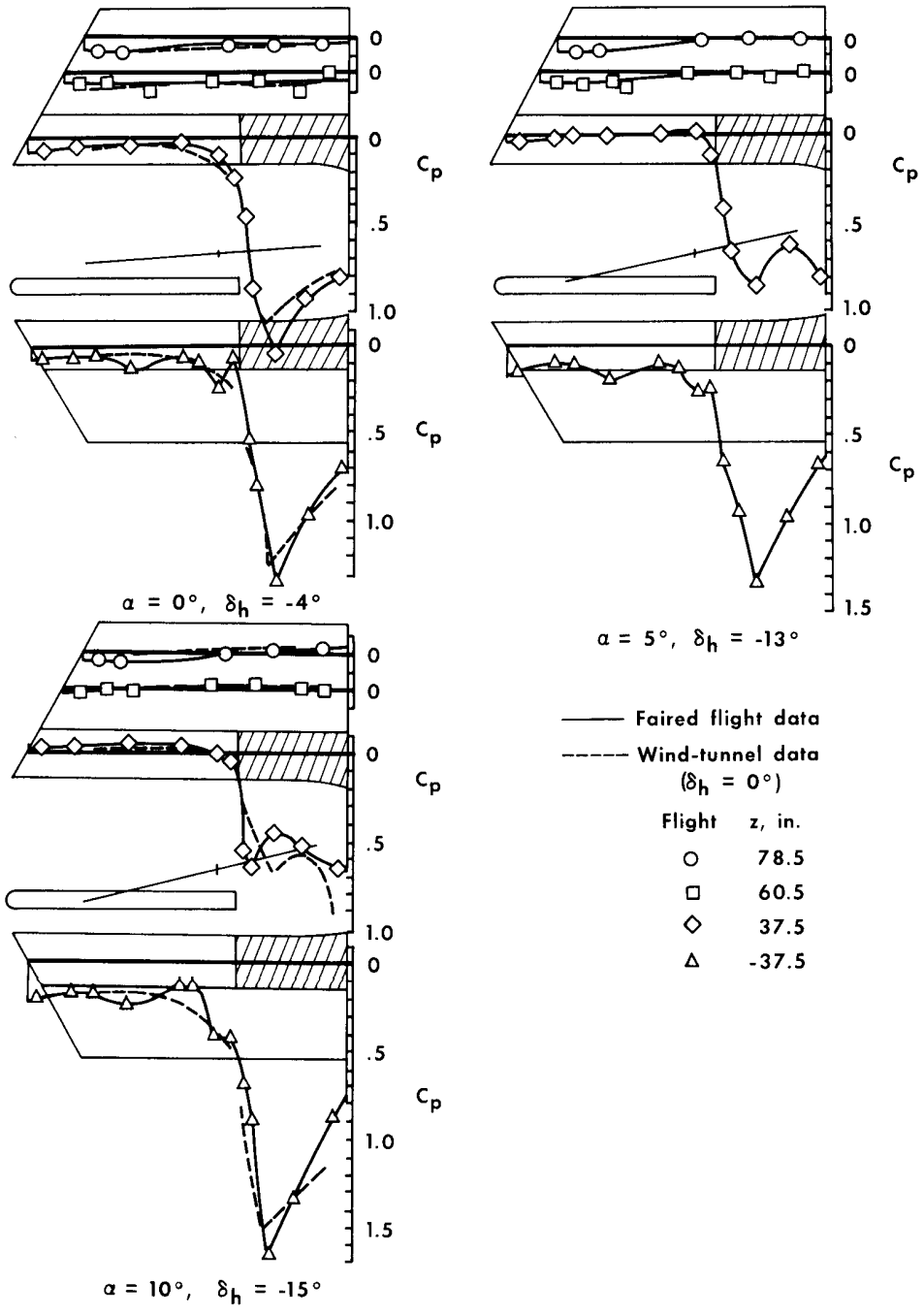

(d) M = 3.0, δ_{SB} = 35°.

Figure 5.- Continued.

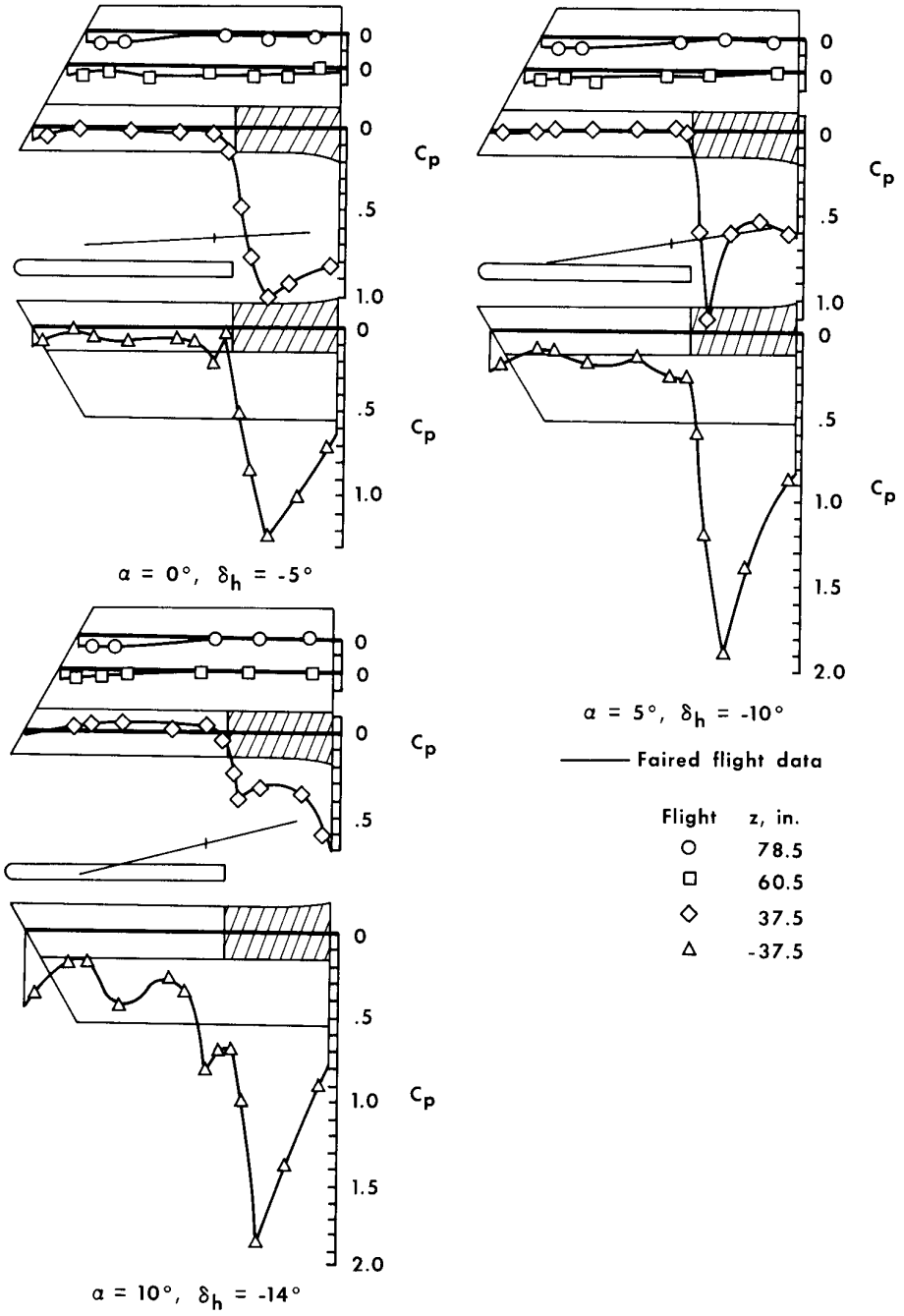

(e) M = 4.0, $\delta_{SB} = 35°$.

Figure 5.– Continued.

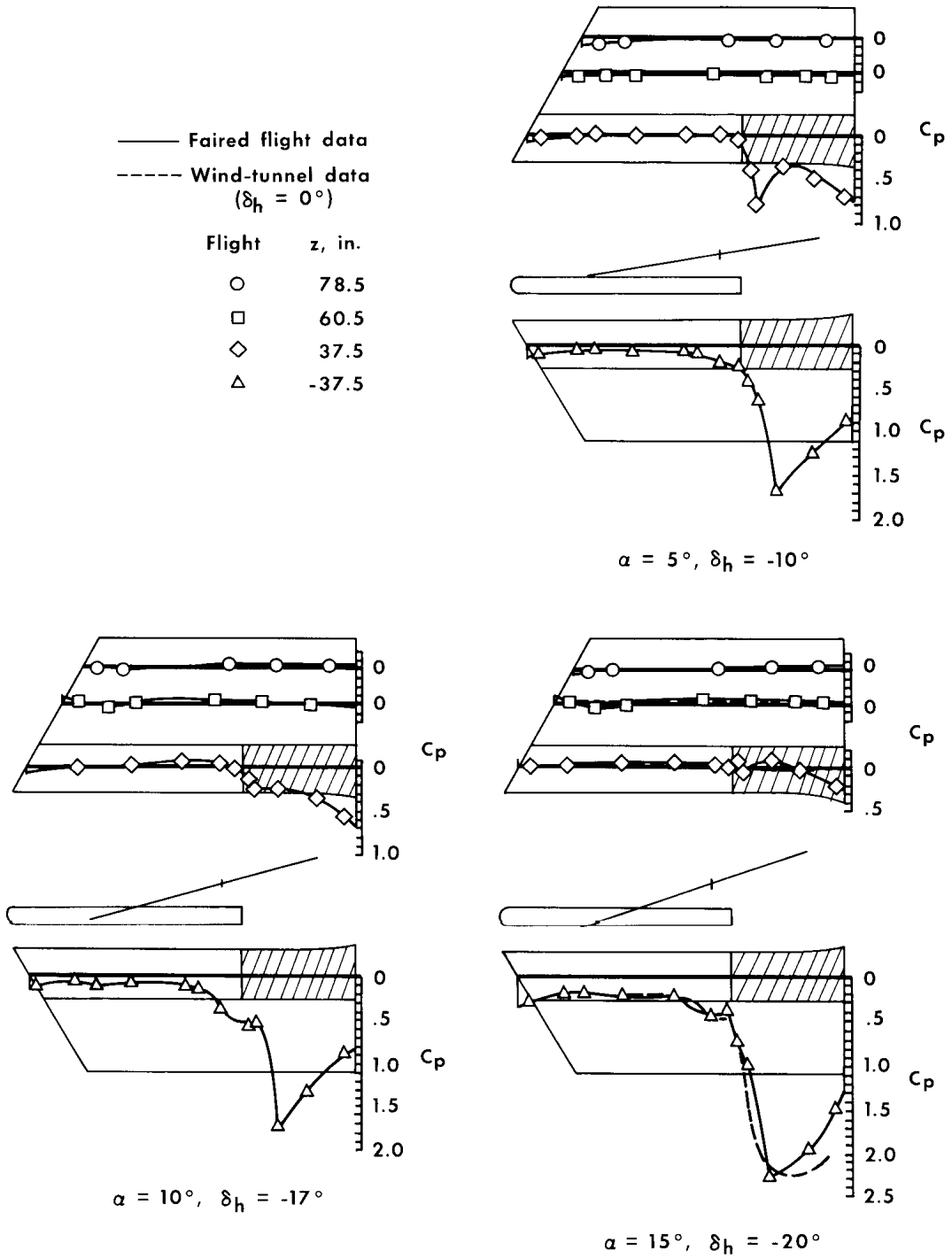

(f) M = 4.7, δ_{SB} = 35°.

Figure 5.– Continued.

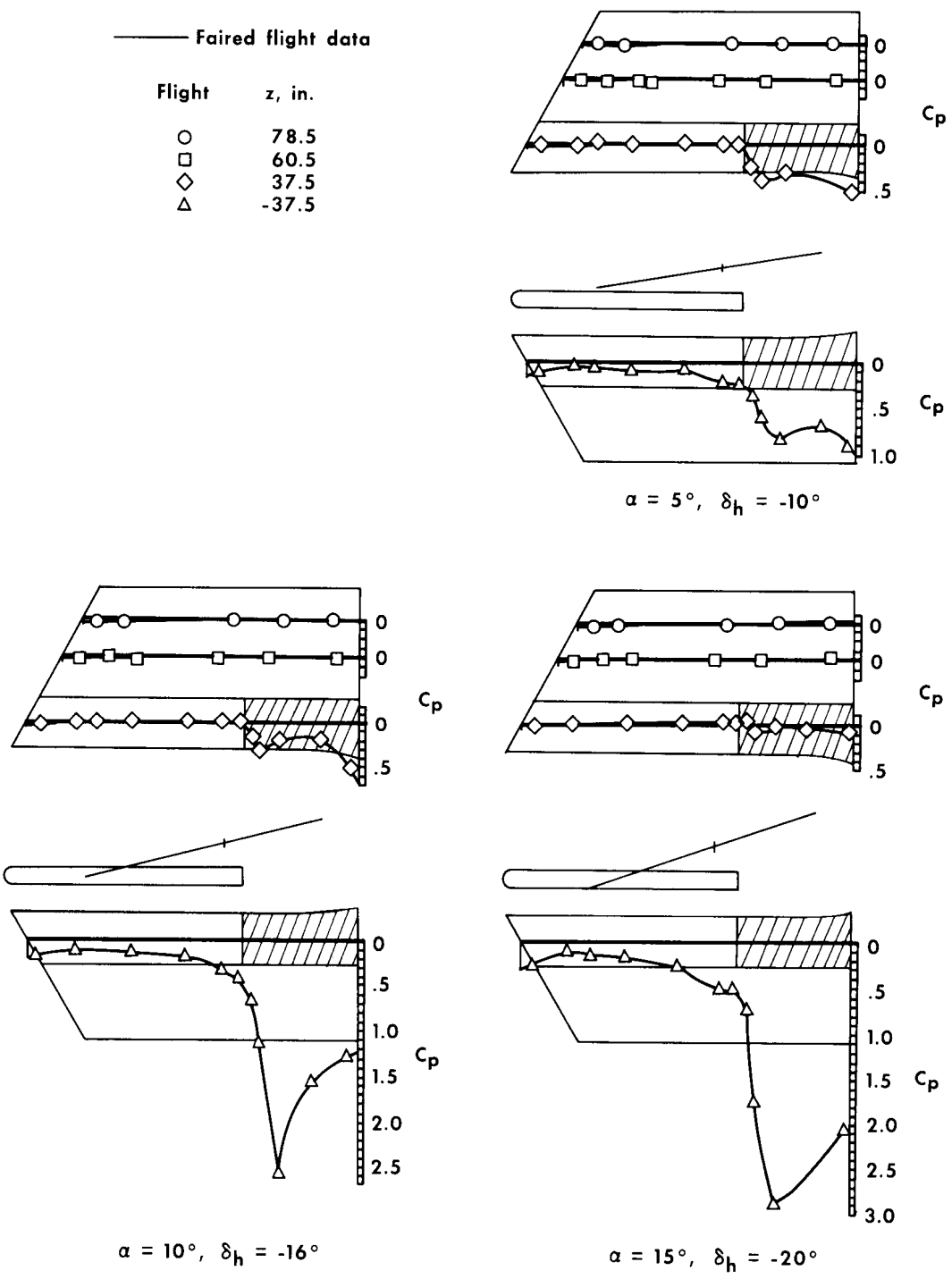

(g) M = 5.2, δ_{SB} = 35°.

Figure 5.– Concluded.

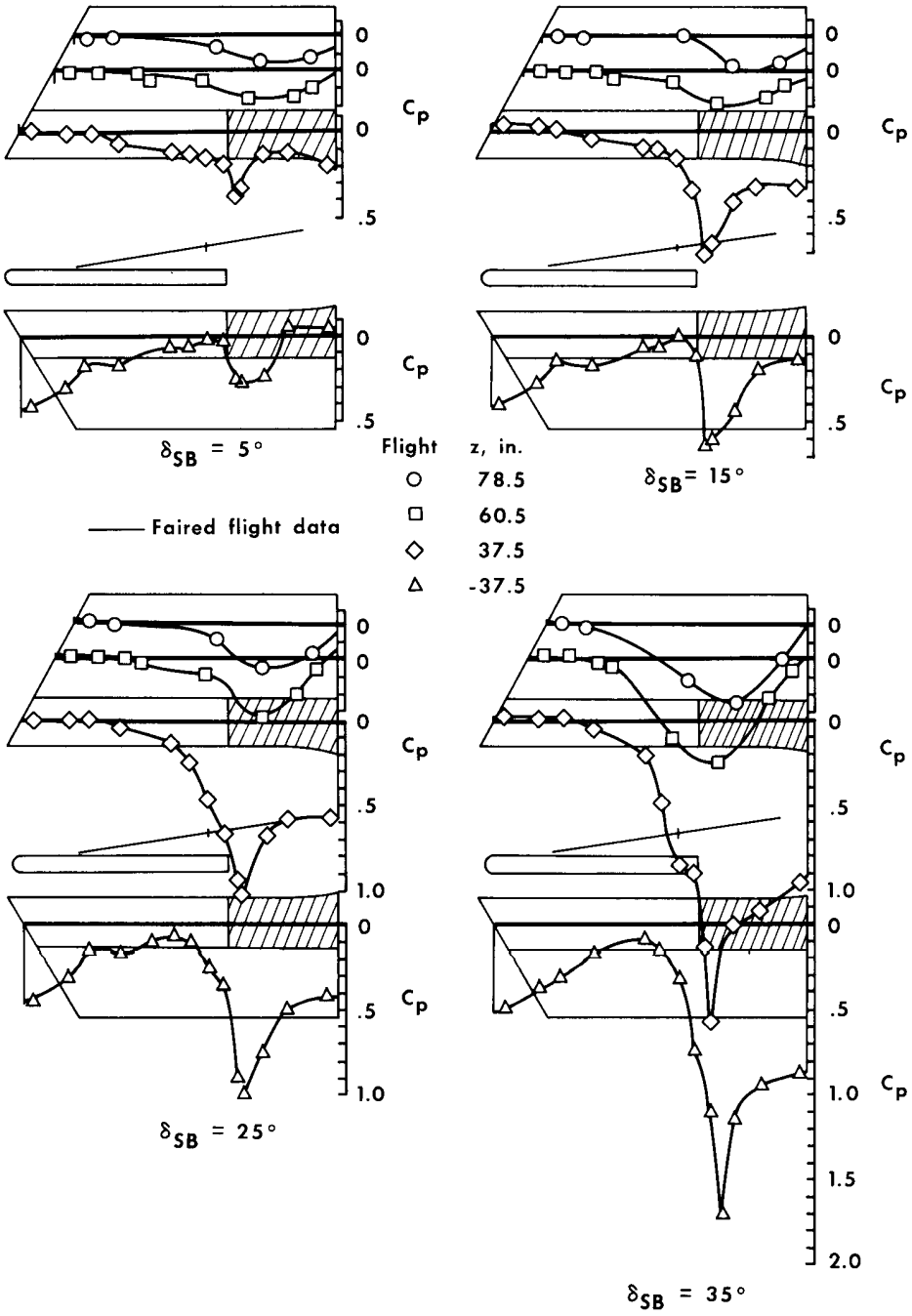

(a) M = 1.4, $\alpha = 5°$, $\delta_h = -9°$.

Figure 6.– Flight-measured surface-pressure measurements on the vertical stabilizers for four speed-brake deflections.

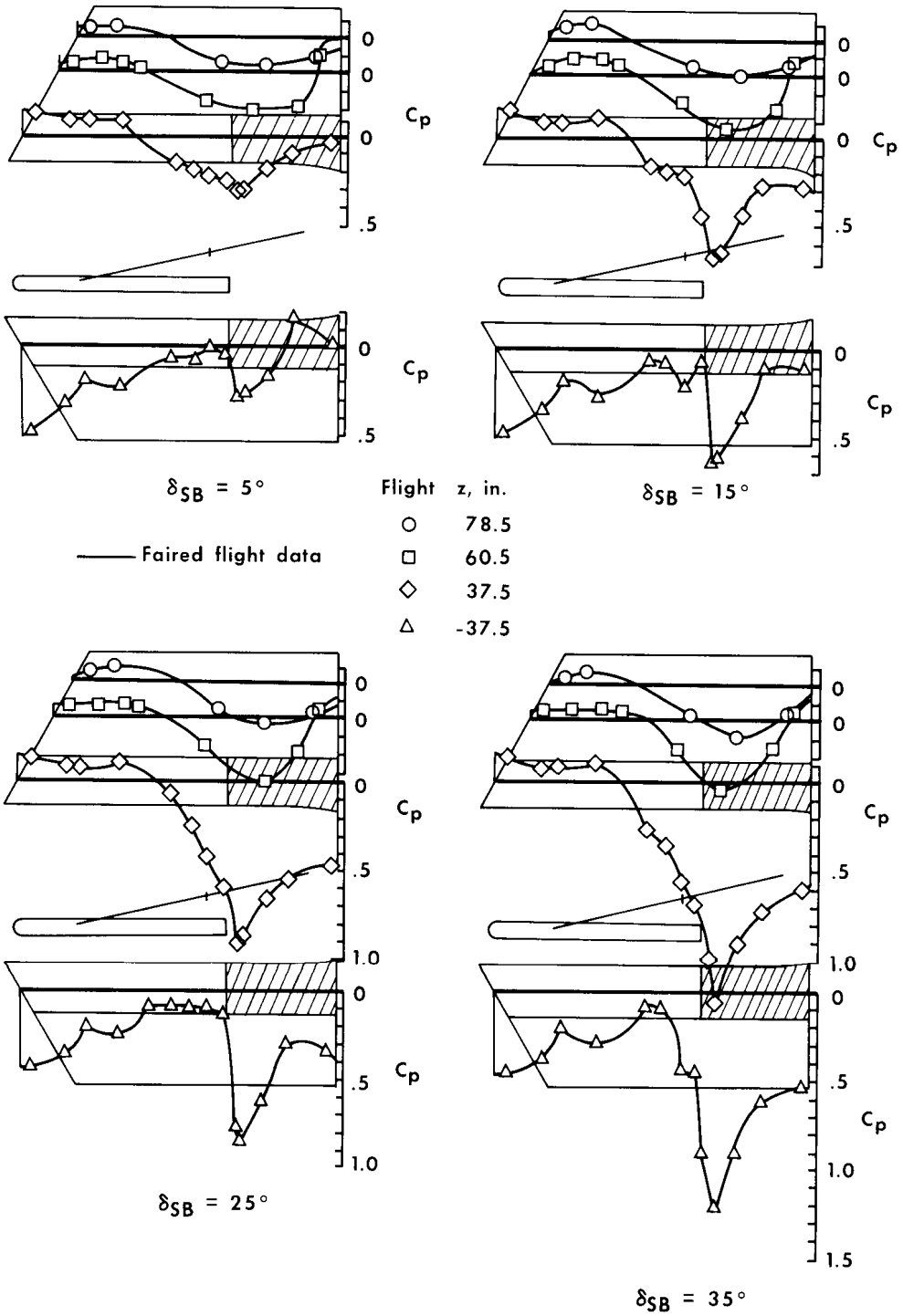

(b) M = 1.4, α = 10°, δ_h = -12°.

Figure 6.– Continued.

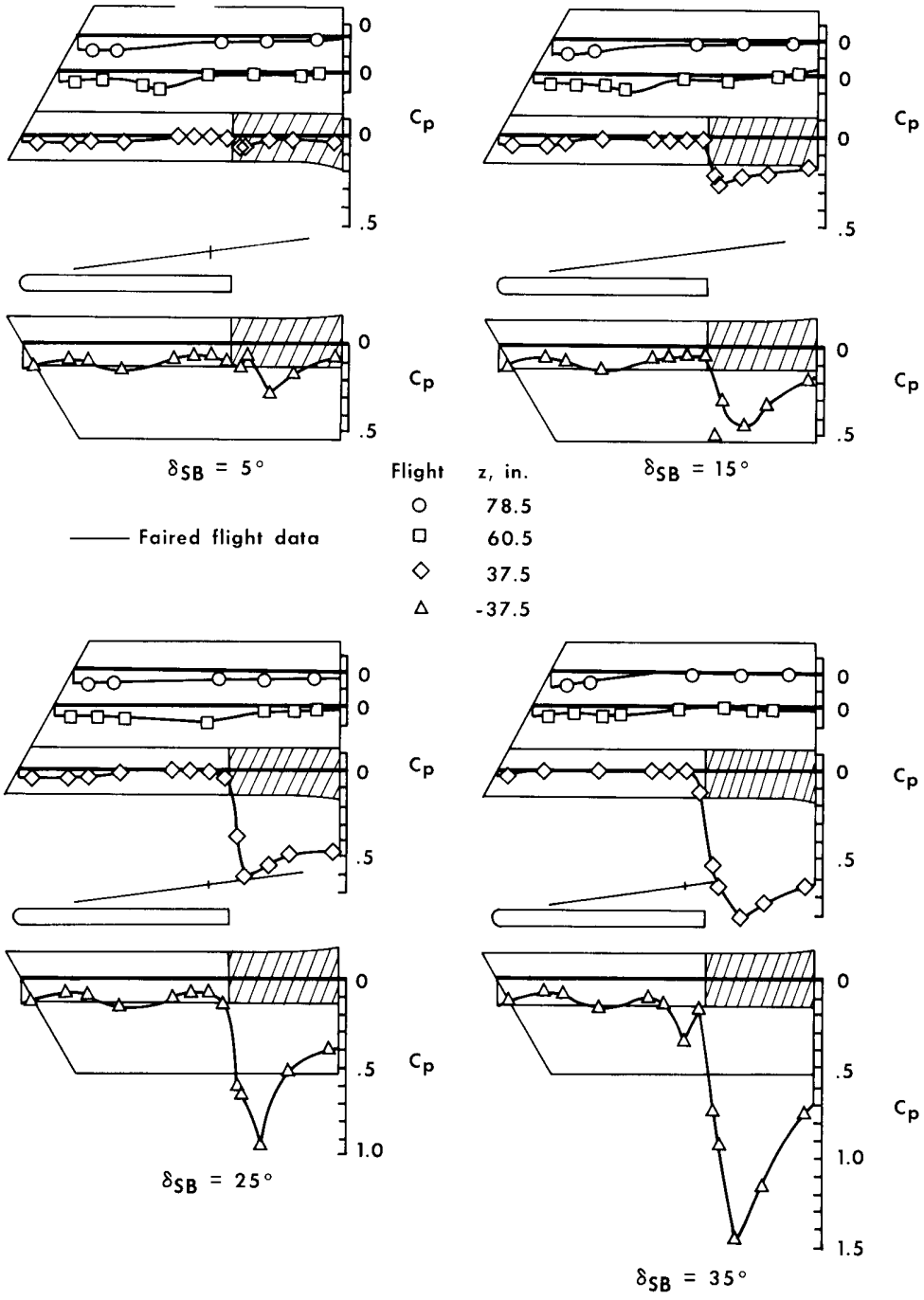

(c) M = 3.0, $\alpha = 5°$, $\delta_h = -8°$.

Figure 6.– Continued.

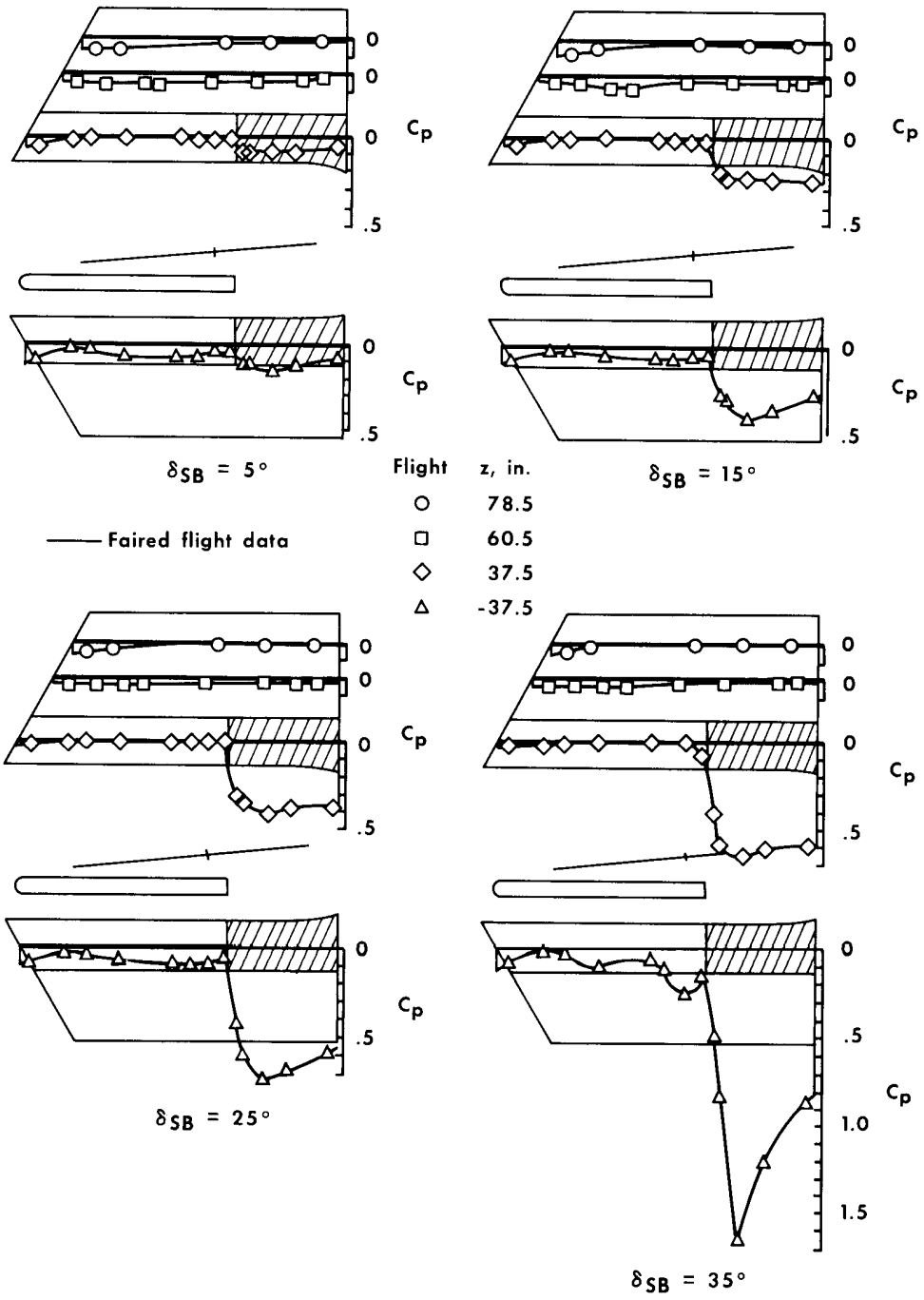

(d) M = 4.5, $\alpha = 5°$, $\delta_h = -5°$.

Figure 6.– Continued.

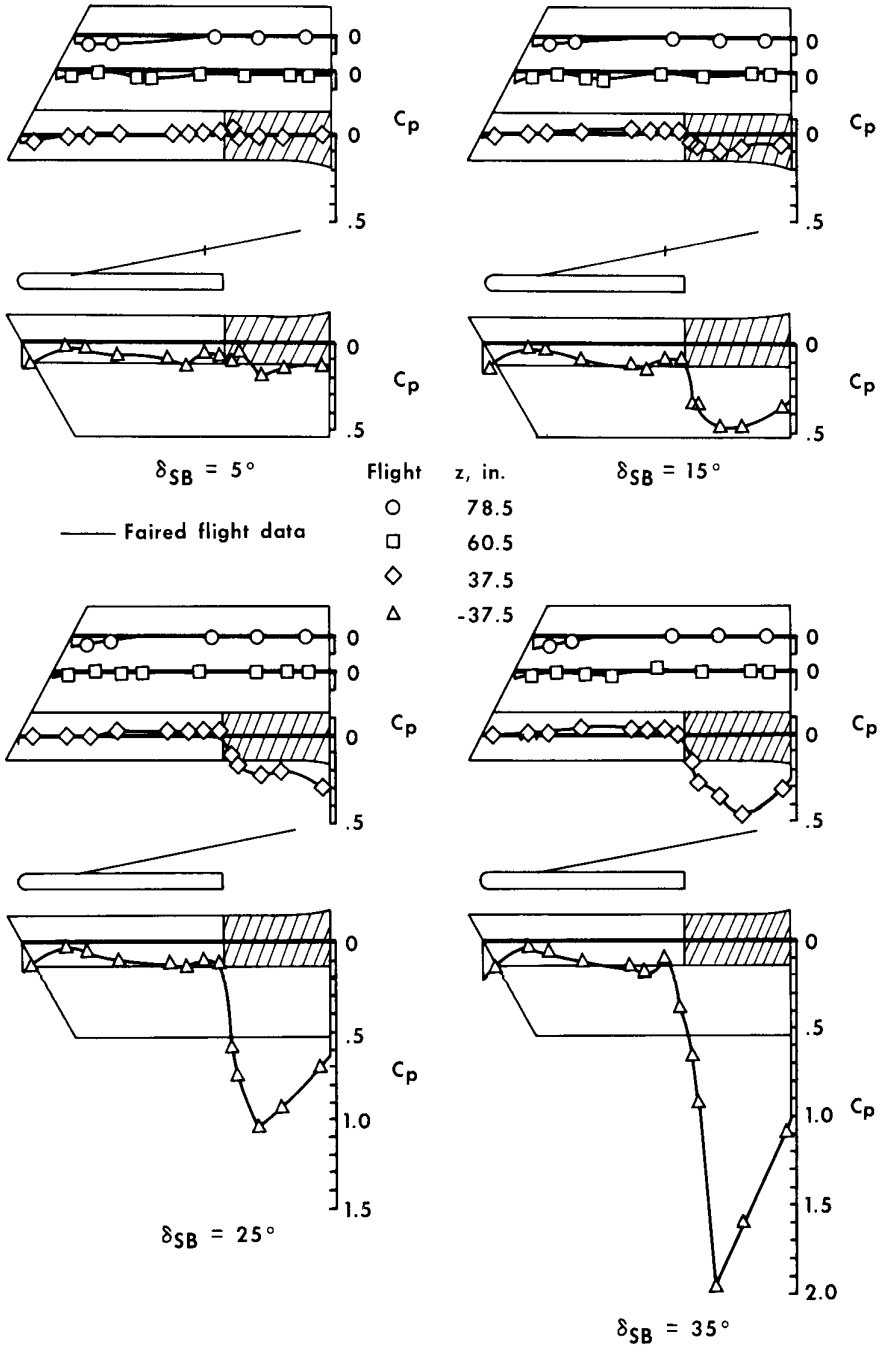

(e) M = 4.5, α = 10°, δ_h = -11°.

Figure 6.- Concluded.

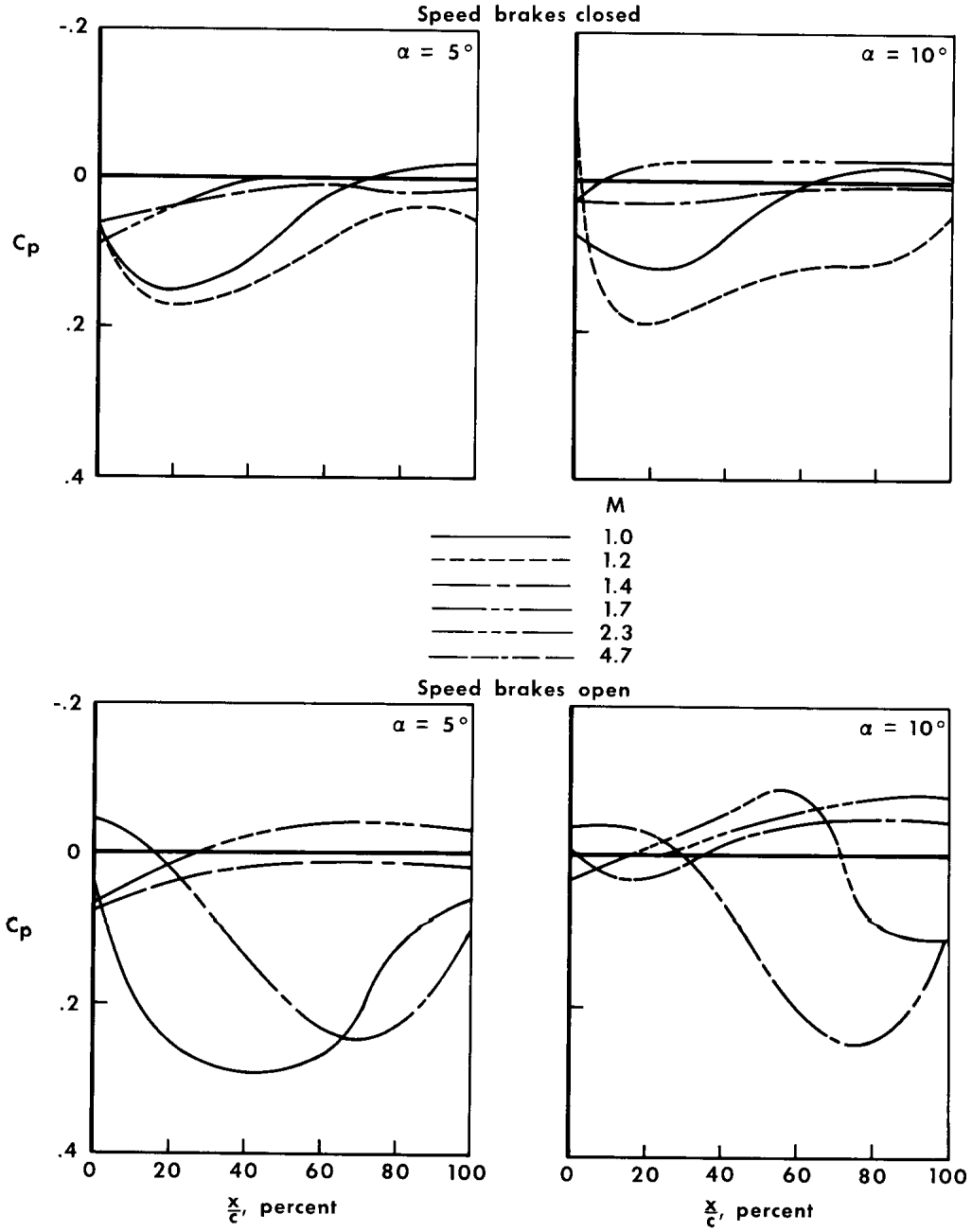

(a) Top row.

Figure 7.– Effect of Mach number and angle of attack on pressure coefficients on the vertical stabilizers.

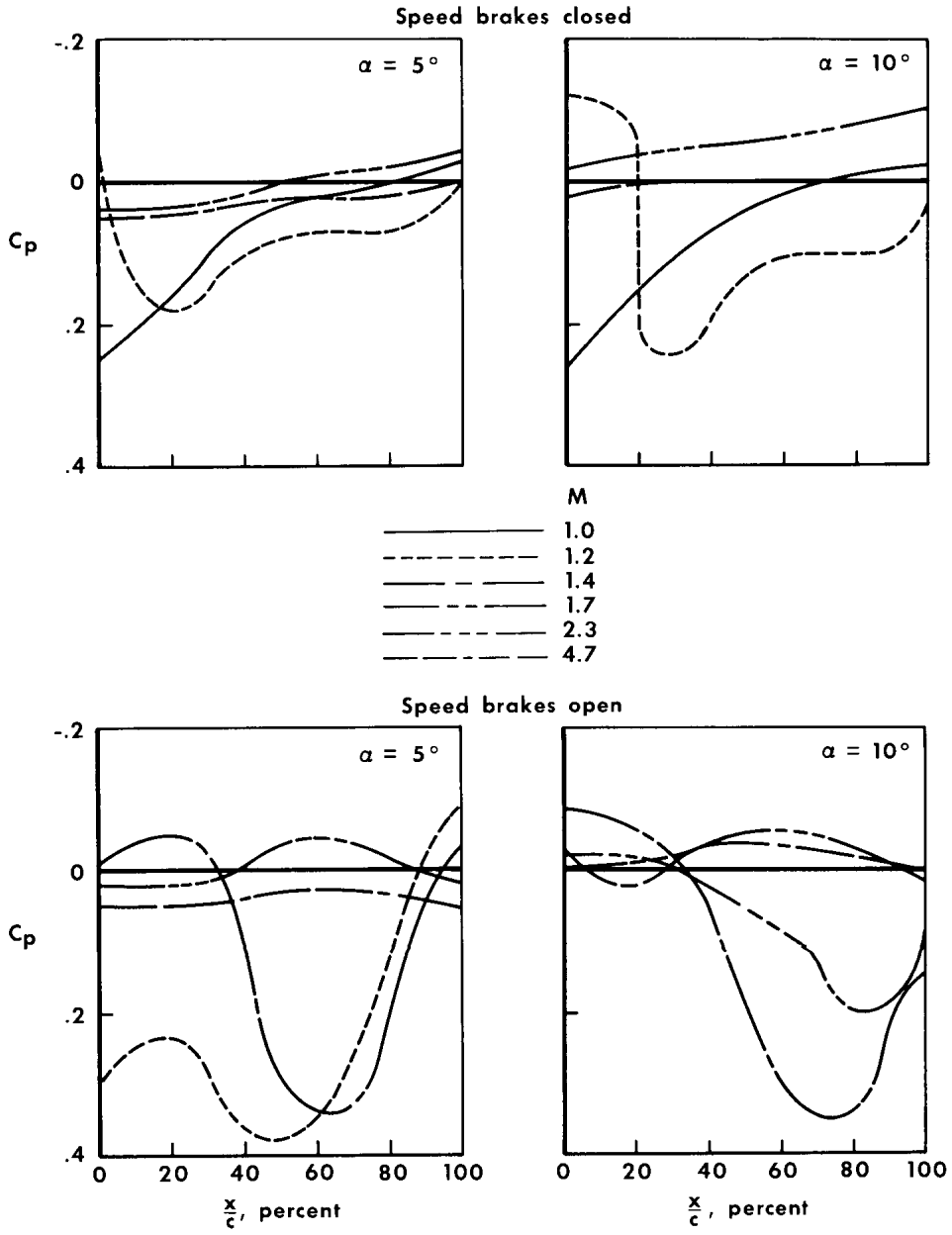

(b) Middle row.

Figure 7.– Continued.

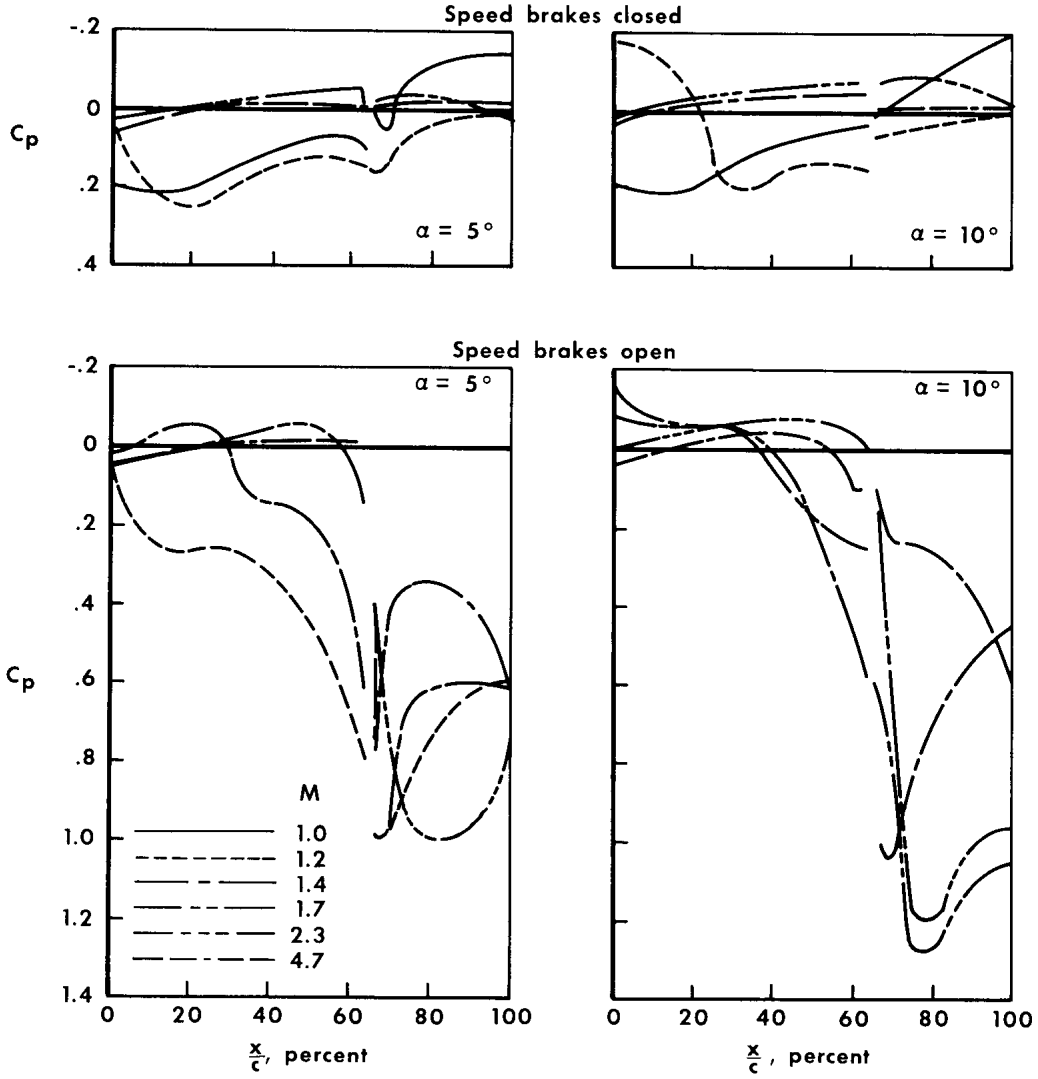

(c) Upper root row.

Figure 7.– Continued.

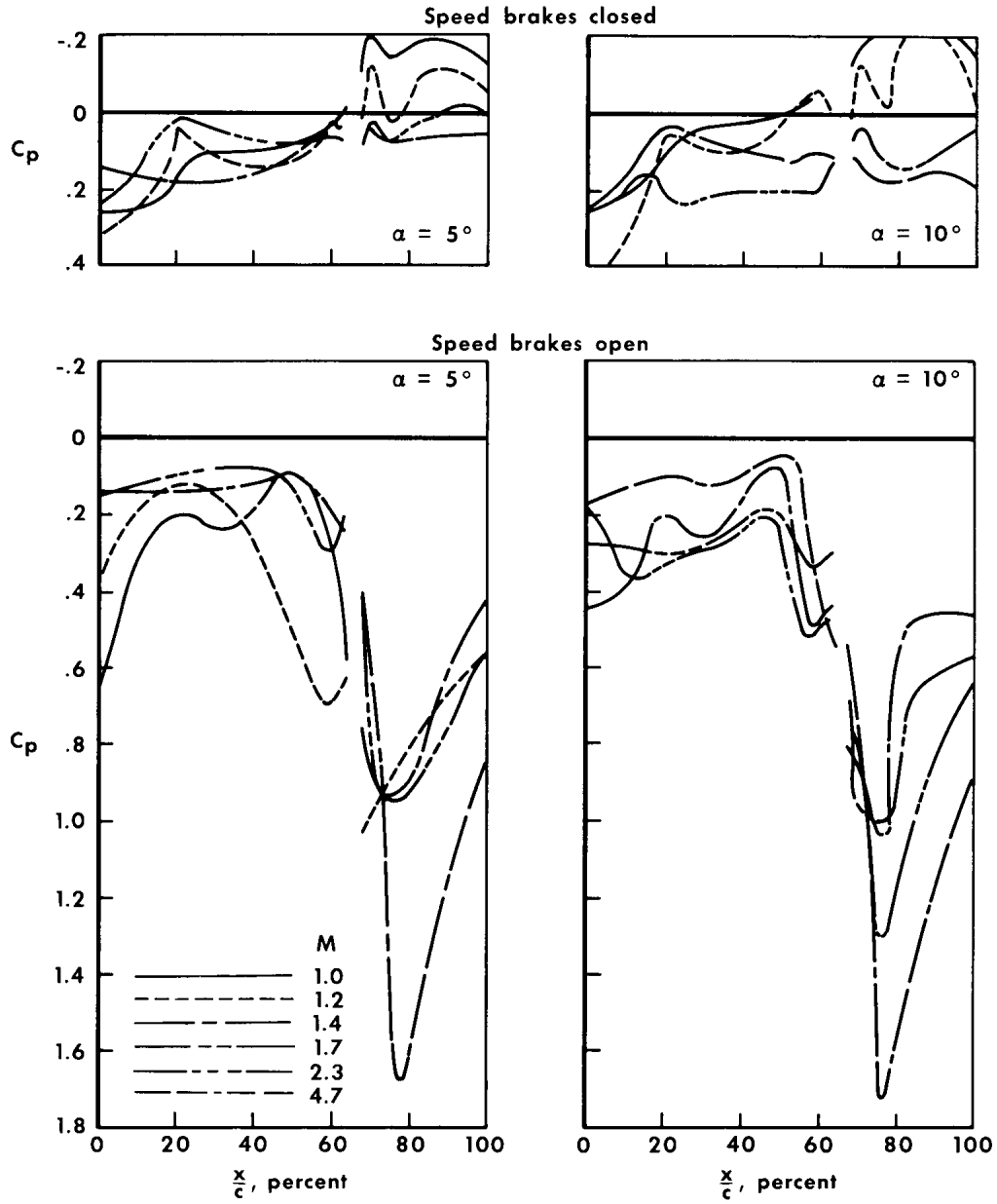

(d) Lower root row.

Figure 7.– Concluded.

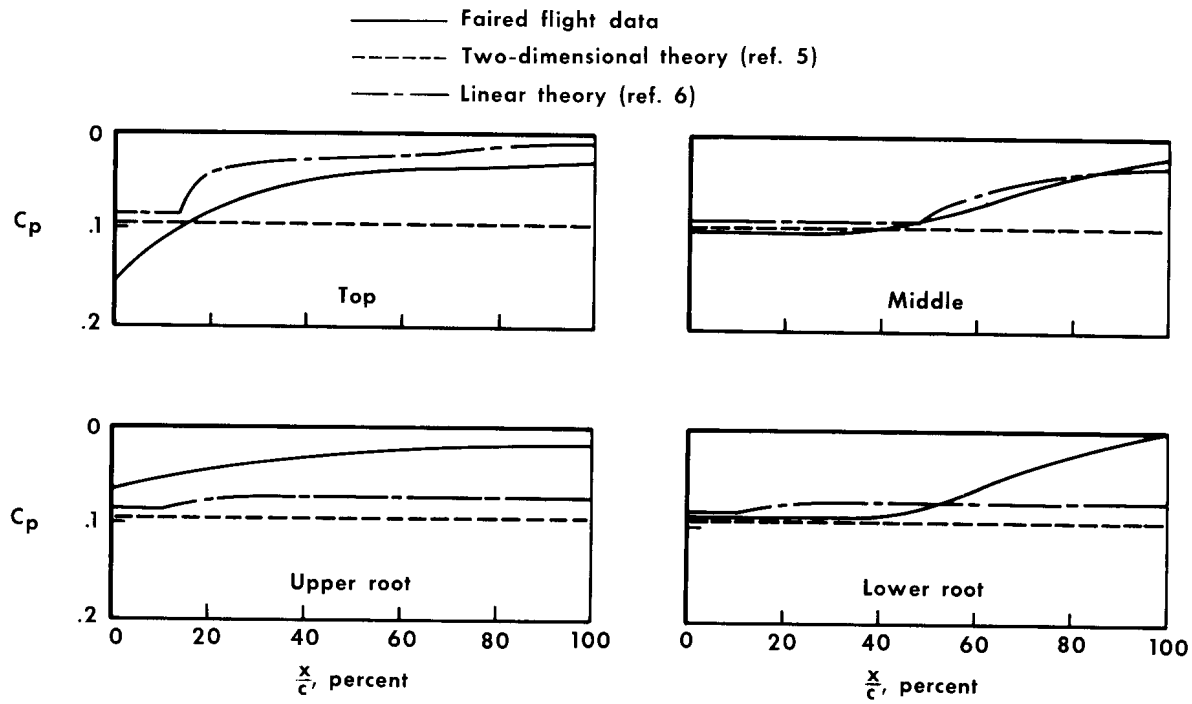

(a) M = 2.3, $\alpha = 0°$, $\delta_{SB} = 0°$.

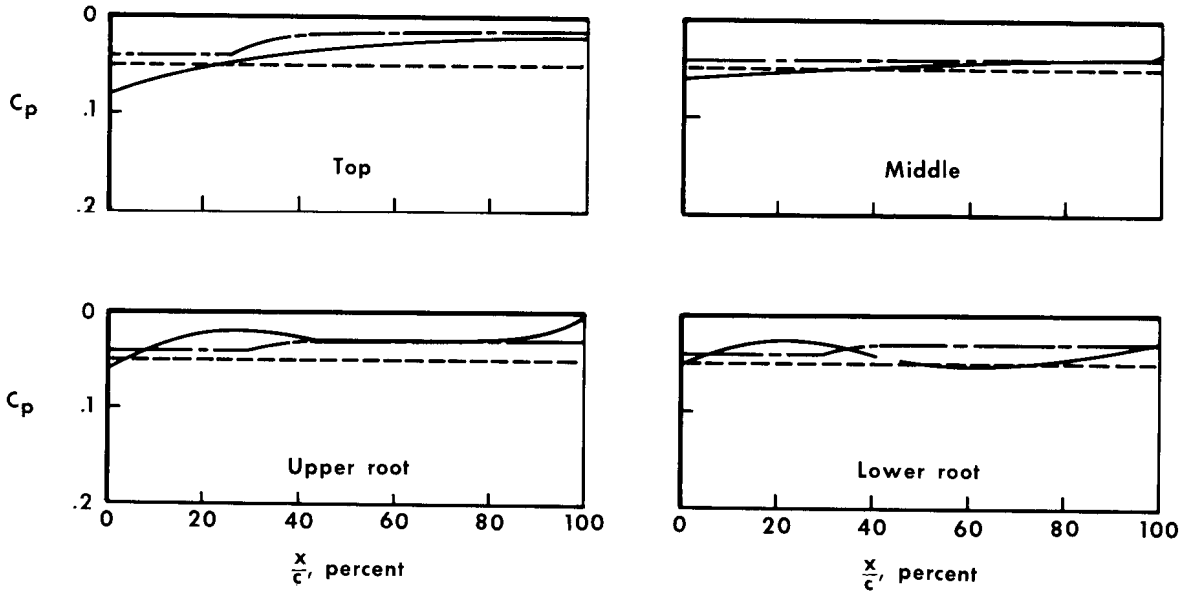

(b) M = 4.7, $\alpha = 0°$, $\delta_{SB} = 0°$.

Figure 8.- Comparison of flight data with theoretical predictions at four spanwise locations.

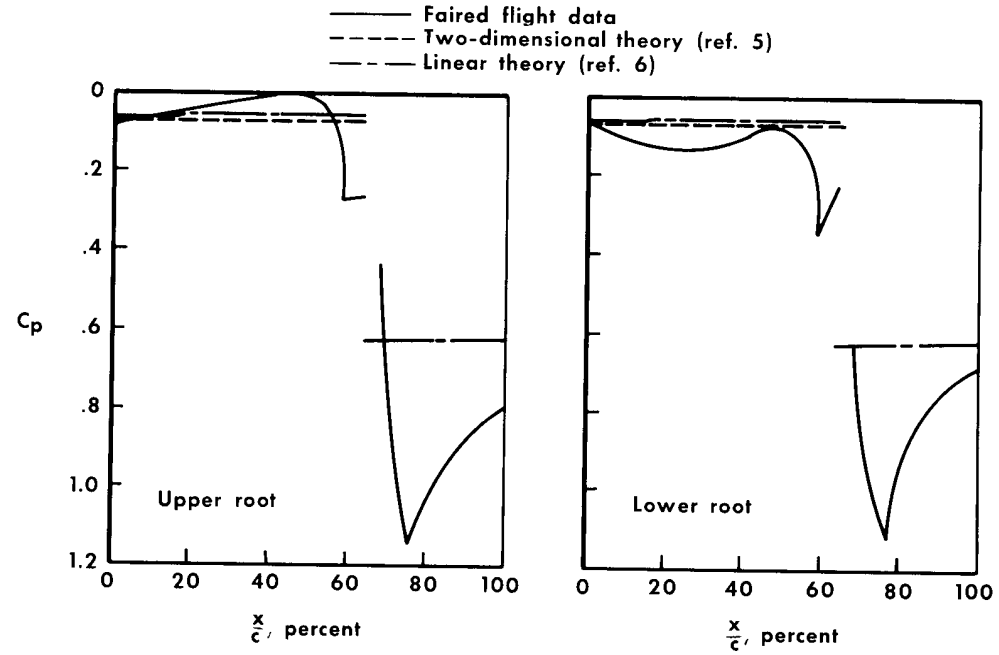

(c) M = 2.3, $\alpha = 0°$, $\delta_{SB} = 35°$.

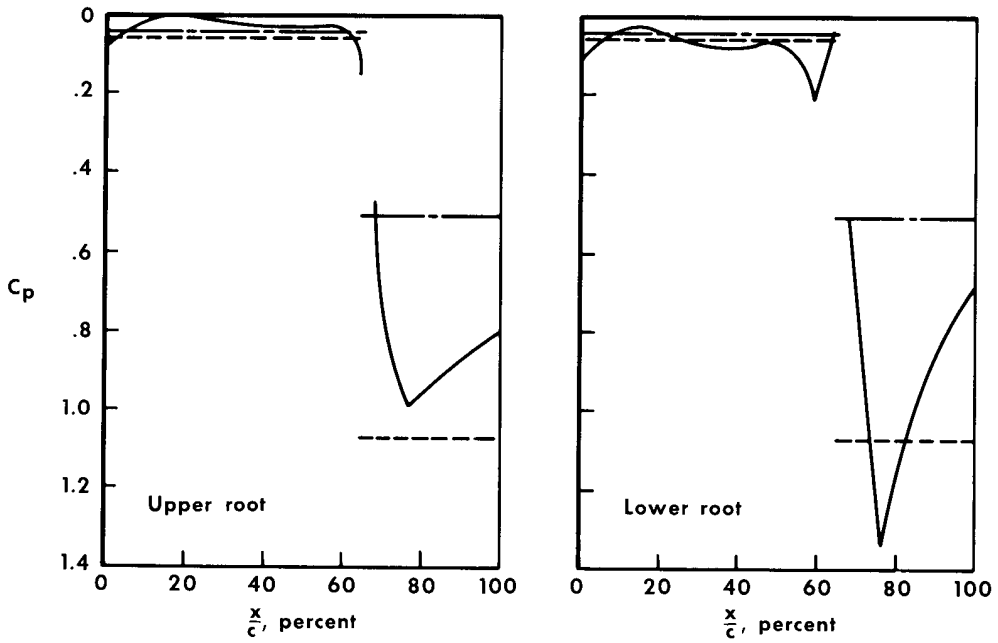

(d) M = 4.0, $\alpha = 0°$, $\delta_{SB} = 35°$.

Figure 8.– Concluded.

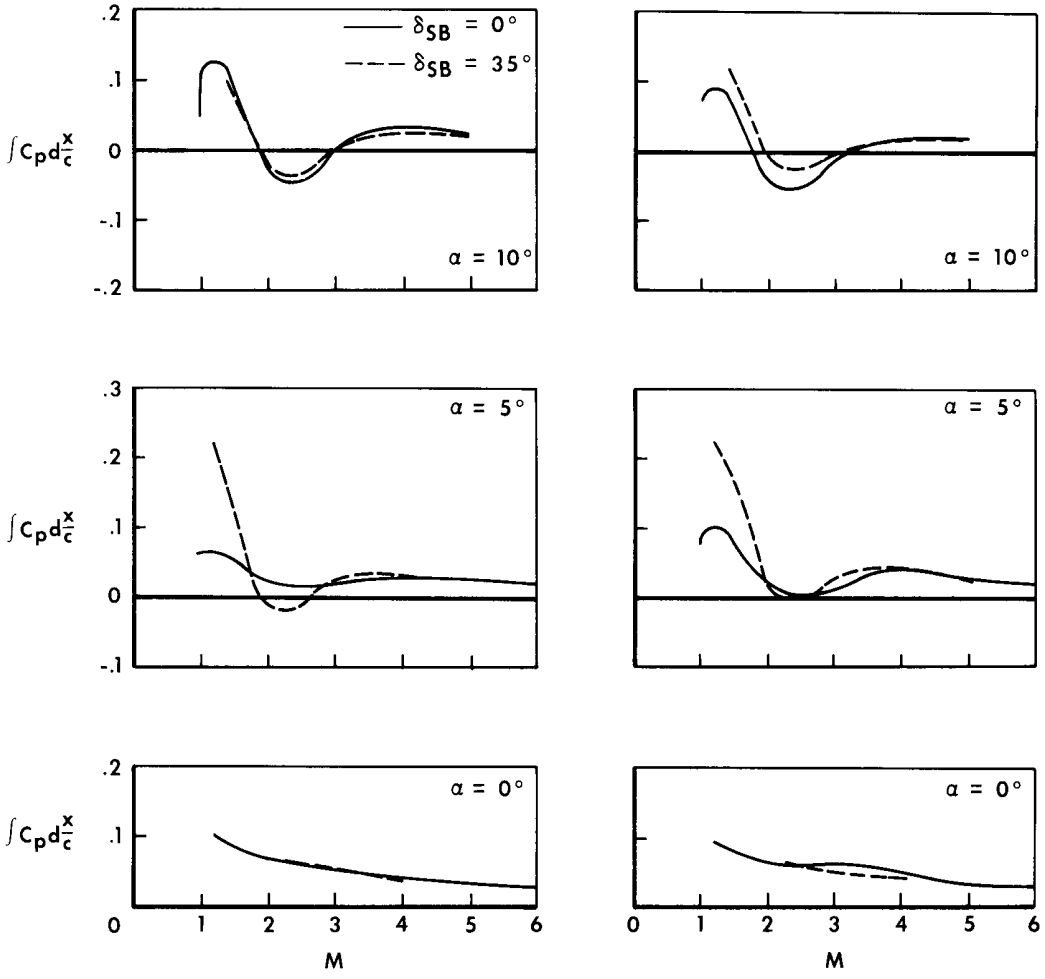

(a) Top row.

(b) Middle row.

Figure 9.– Effect of speed-brake chordwise load on the vertical stabilizers as a function of Mach number.

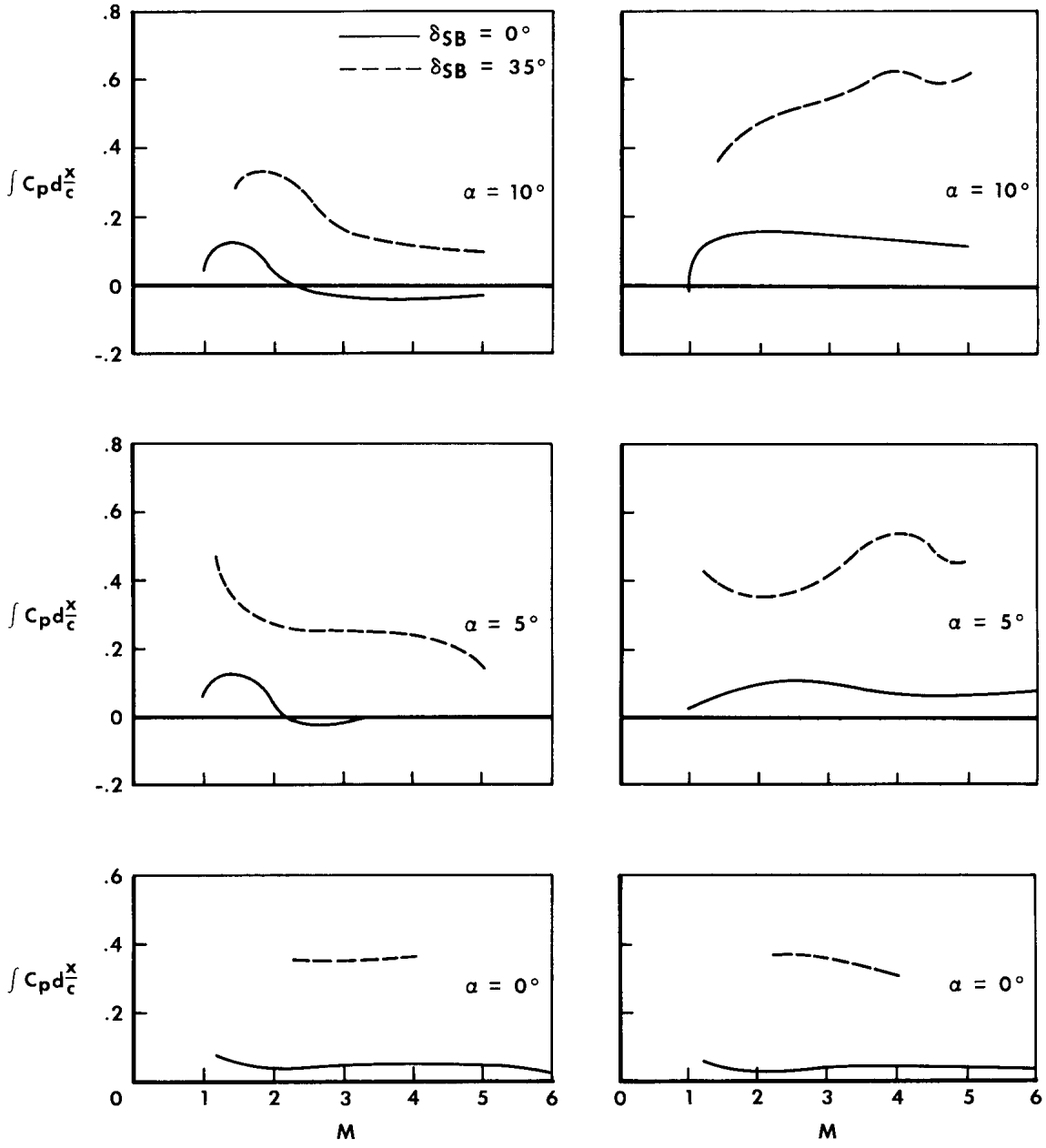

(c) Upper root row.

(d) Lower root row.

Figure 9.– Concluded.

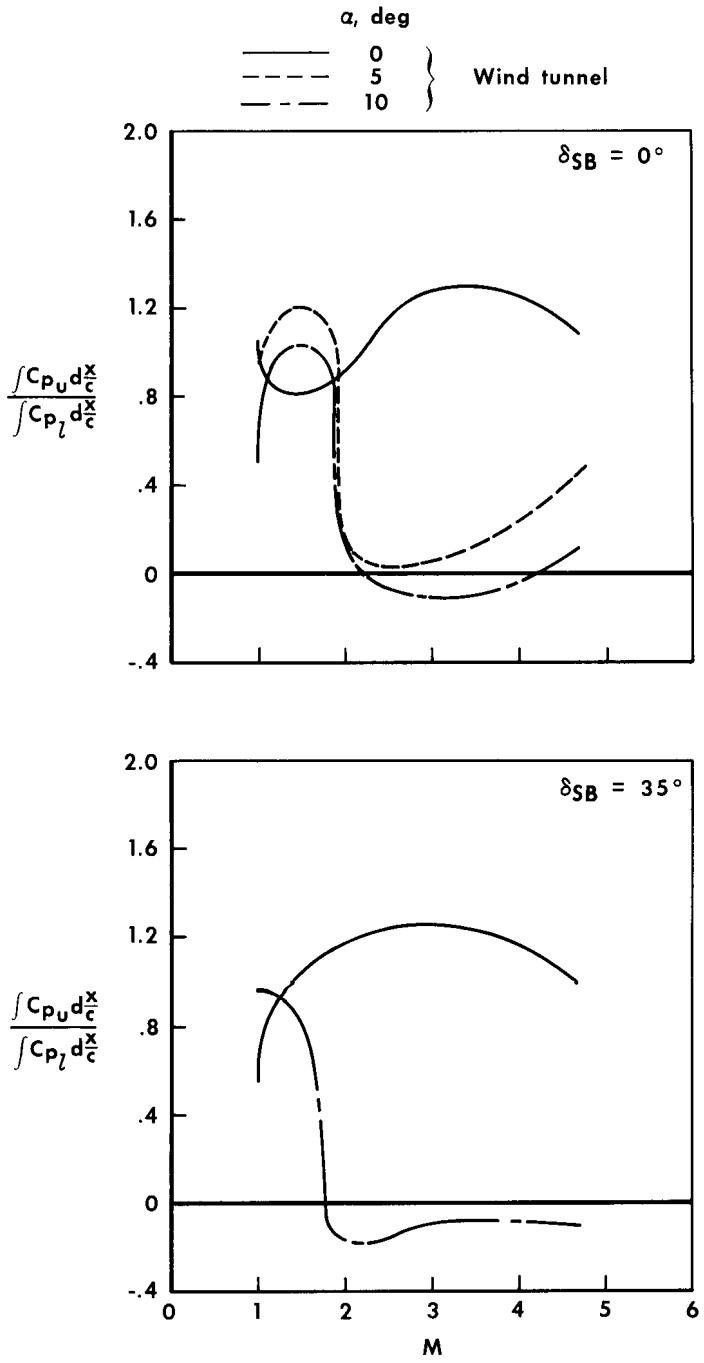

Figure 10.- Effectiveness of the movable control surfaces.

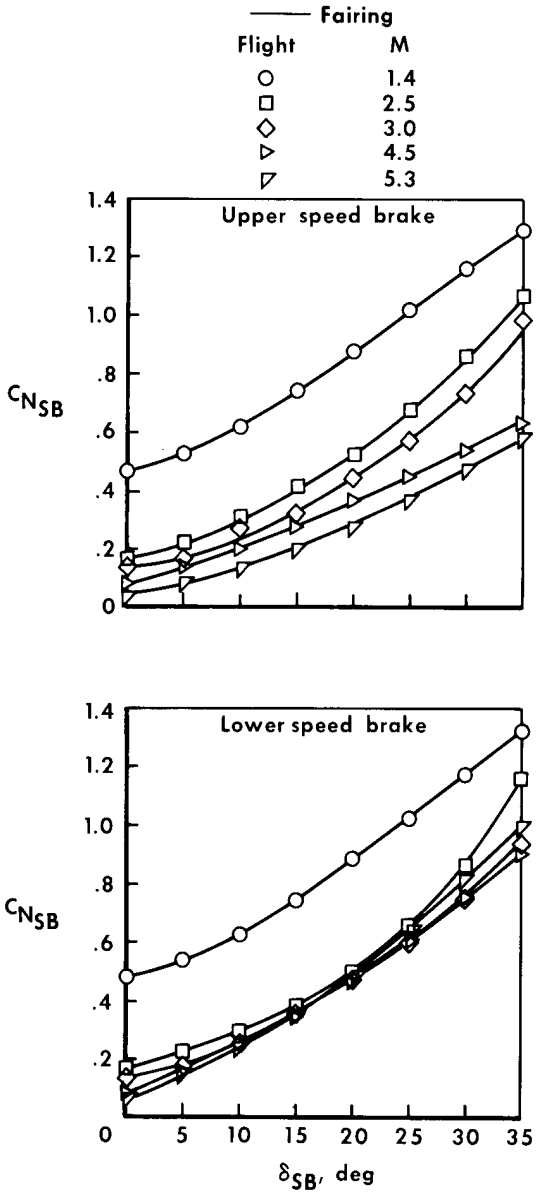

Figure 11.- Increase in normal-force coefficient caused by deflection of speed brakes. $\alpha = 5°$.

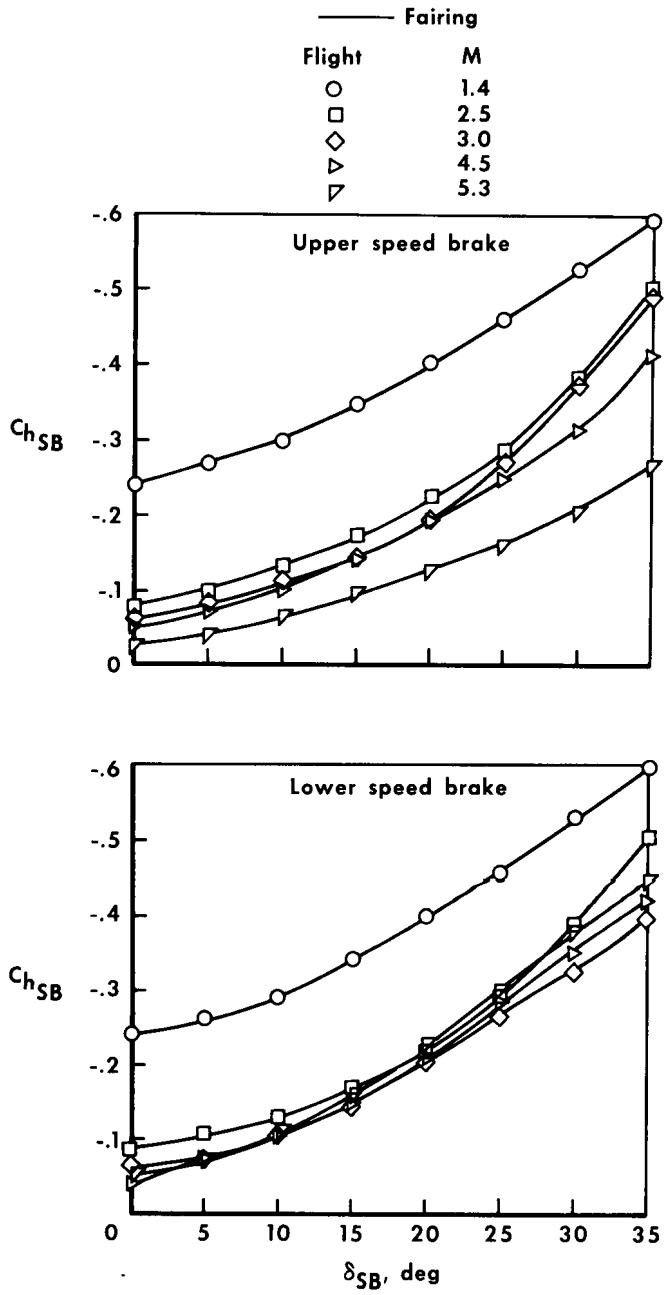

Figure 12.– Increase in hinge-moment coefficient caused by deflection of speed brakes. $\alpha = 5°$.

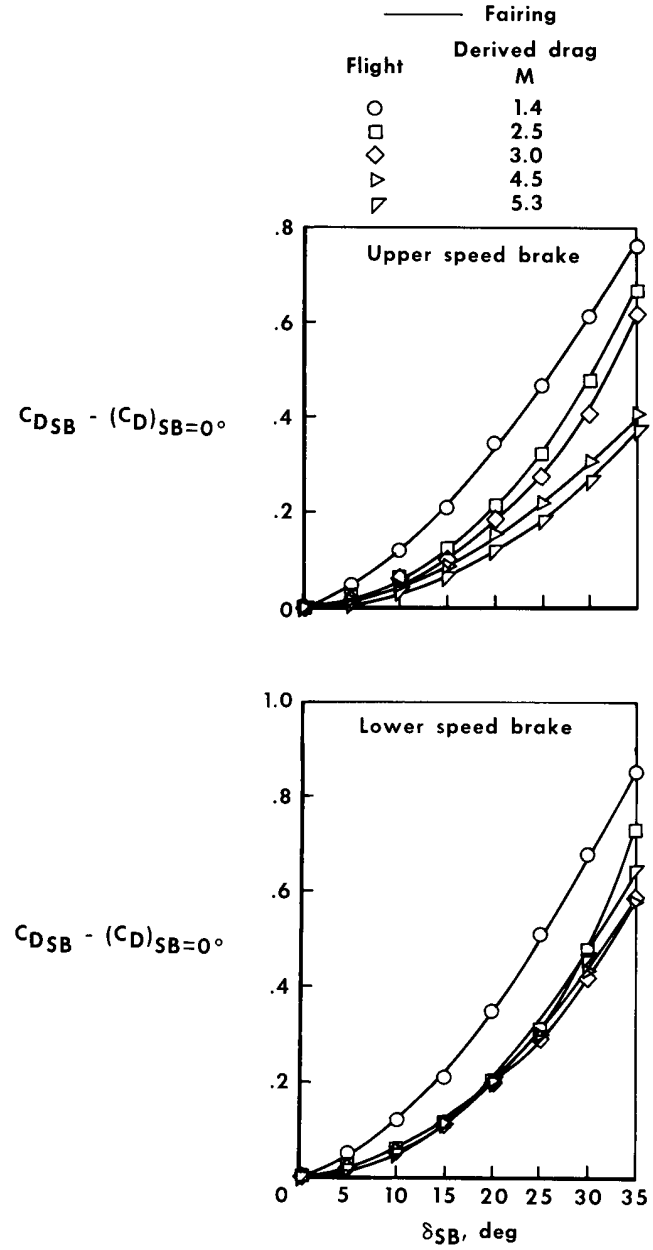

Figure 13.– Increase in surface-pressure drag coefficient caused by deflection of speed brakes. $\alpha = 5°$.

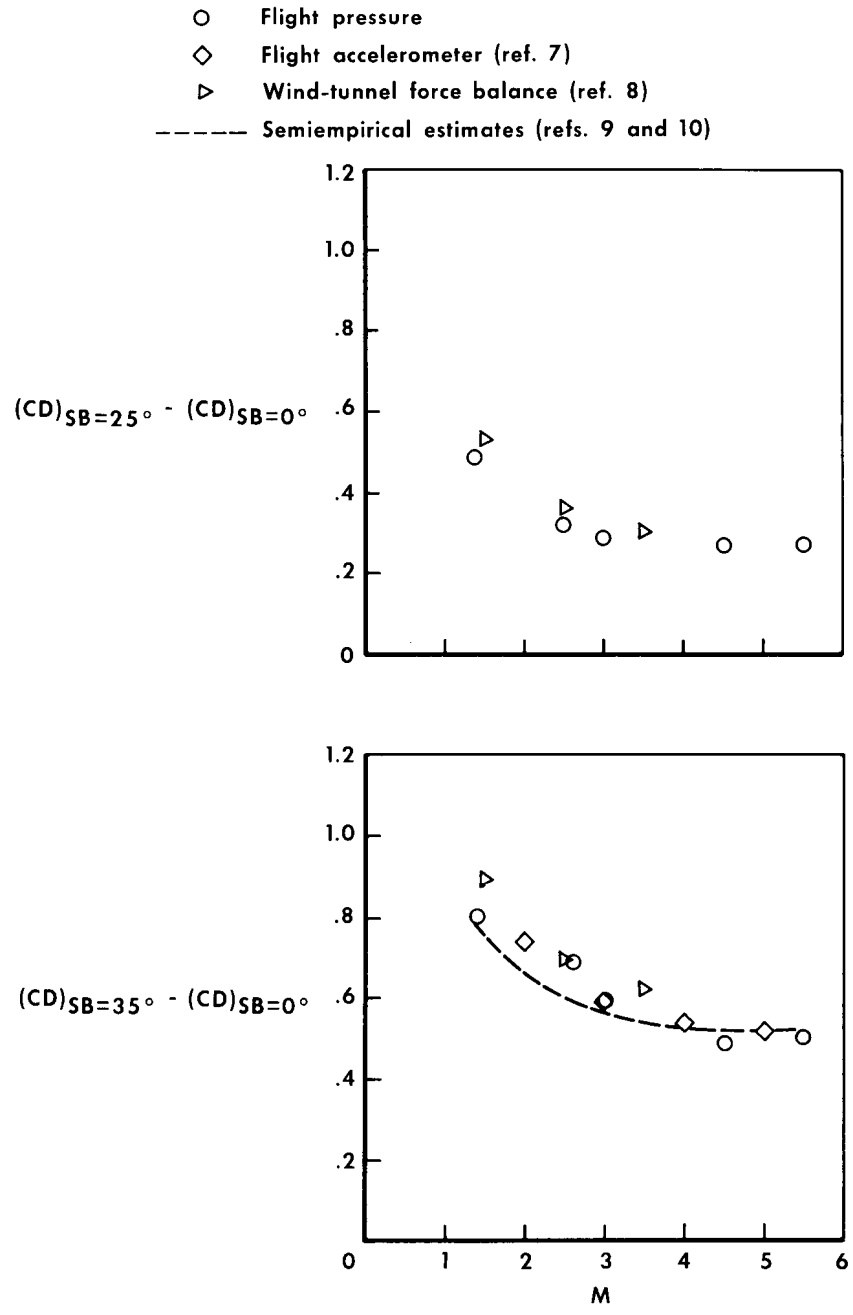

Figure 14.– Comparison of pressure-measured drag with accelerometer, force-balance, and semiempirical drag.